5-2019

Geochemical Analysis of Mississippian Cherts and Devonian-Mississippian Novaculites, Southern Midcontinent Region

Julie Mary Cains
University of Arkansas, Fayetteville

Geochemical Analysis of Mississippian Cherts and Devonian-Mississippian Novaculites, Southern Midcontinent Region

A thesis submitted in partial fulfillment
of the requirements for the degree of
Master of Science in Geology

by

Julie Mary Cains
University of Arkansas
Bachelor of Science in Geology, 2016
University of Arkansas
Bachelor of Arts in Studio Art, 2016

May 2019
University of Arkansas

This thesis is approved for recommendation to the Graduate Council

_____
Walter L. Manger, Ph.D.
Thesis Director

_____
Adriana Potra, Ph.D.
Committee Member

_____
Thomas A. McGilvery, Ph.D.
Committee Member

ABSTRACT

This study uses trace elements and radiogenic isotopes (Pb, Sr, and Nd) to investigate the origin and mode of formation for the siliceous deposits in the Lower Mississippian Boone Formation and the Devonian-Mississippian Arkansas Novaculite in the southern midcontinent. Mississippi Valley-type Pb-Zn ore deposits in the Tri-State District and the Northern Arkansas District were deposited by hydrothermal fluids, and highly radiogenic Pb isotope ratios suggest a genetic relationship between the Boone Formation chert ($^{206}Pb/^{204}Pb \sim 21.59$, $^{207}Pb/^{204}Pb \sim 15.87$, $^{208}Pb/^{204}Pb \sim 40.10$) and the MVT ores. Due to the very low concentration of Pb in the Boone chert (~2 ppm) and the close proximity of samples containing radiogenic Pb to the tripolitic chert interval, the Boone Formation is interpreted to have been contaminated with radiogenic Pb by the hydrothermal fluids that emplaced the ores. Calculated epsilon values for Nd reveal a small positive shift in the Boone samples (ε Nd ~ -5.5) relative to other measured stratigraphic intervals in the southern midcontinent (ε Nd ~ -15.2), potentially indicating volcanic contribution of Nd. Upper Boone cherts (ε Nd ~ -4.6) and Hatton Tuff (ε Nd ~ -3.8) values are remarkably similar, indicating the same Nd source. Sr isotope ratios of the Boone samples ($^{87}Sr/^{86}Sr \sim 0.7089$) largely reflect Mississippian seawater Sr ($^{87}Sr/^{86}Sr \sim 0.7080$), while the novaculite samples contain more radiogenic Sr ($^{87}Sr/^{86}Sr \sim 0.7121$), likely reflecting Sr exchange from the detrital component within the Arkansas Novaculite stratigraphic interval. Rare earth element (REE) concentrations normalized to average continental arcs plot near one for the upper Boone chert samples, indicating similar compositions, while the lower Boone and Arkansas Novaculite have lower normalized values. Rare earth element plus yttrium (REY) concentrations normalized to Post-Archean Australian Shales (PAAS) reveal a negative cerium (Ce) anomaly and a positive yttrium (Y) anomaly, which is a signature of seawater, indicating that the Boone cherts may retain a depositional seawater REY signature.

ACKNOWLEDGEMENTS

First, I have to thank my father, Bill Cains, for sharing his love of geology and the outdoors with me throughout my entire life, and for taking me on so many adventures learning about geology by boat, by foot, by maps, or by books. You are the reason I am a geologist.

I also owe a great debt of gratitude to my mentor and inspiration, Dr. Walter Manger. I vividly remember the awe-struck feeling I had while sitting on the banks of the Colorado River, listening to Dr. Manger read from John Wesley Powell's journal detailing his journey through the Grand Canyon. Dr. Manger instilled in me a deep appreciation for stratigraphy, as well as a great sense of respect for the history of geology and all the work that has been done to advance our science. I'll always remember "the essence of education is the conquest of parochialism."

I would also like to thank Dr. Adriana Potra for her friendship and her patience throughout this research project. She has taught me everything I know about geochemistry and has inspired me to venture out of my comfort zone. Dr. Potra has been a guiding light throughout every step of this process, and I'm grateful for all she has taught me. I'd like to thank John Samuelsen for the many hours he spent helping me run all of my isotope analyses on the multicollector. I also thank Erik Pollock and Barry Shaulis for all of their time and effort devoted to analyzing my samples. My deepest thanks go to the one and only Mac McGilvery for returning to Arkansas and the University to share his unique perspective that blurs the lines between industry and academia. Mac, you speak my language and inspire me to be my own kind of geologist. A special thank you goes to my mom, Mary Jane, and my siblings, Caroline, Amanda, and Will, for their unceasing support and encouragement throughout this process. I am very lucky to have siblings that share my enthusiasm for sedimentary geology and with whom I can always debate interpretations and ask for advice. Last but not least, I'd like to thank Sydney McKim for being a true friend and always encouraging me throughout this journey.

DEDICATION

I would like to dedicate this thesis to my friends Stephen Denham, Sean Kincade, and Forrest McFarlin for making graduate school such an interesting experience. You may have put my field book in Jell-O, but at least our field trips were never boring.

CONTENTS

LIST OF TABLES

LIST OF FIGURES

1. INTRODUCTION

1.1 Purpose and Scope

The Lower Mississippian interval in northern Arkansas and southern Missouri is a succession of chert-bearing carbonate rocks that are designated the St. Joe and succeeding Boone Formations (McFarland, 1998 (revised 2004). The Devonian-Mississippian Arkansas Novaculite (Griswold, 1892) in the Ouachita region of Arkansas is characterized by thick intervals of bedded novaculite, as well as interbedded shales. The Boone Formation contains both penecontemporaneous and replacement cherts, and it hosts some of the Mississippi Valley-Type ore deposits found in the Northern Arkansas and Tri-state Ore Districts. This study utilizes geochemical data primarily on the siliceous intervals found in both the Boone Formation and the Arkansas Novaculite to evaluate the mode of formation and the silica source for the cherts and novaculite. Trace element and isotope data collected for this thesis provide further insight into the depositional and diagenetic history of this interval, as well as potential sources of the metals comprising the ore deposits. This study further explores the potential genetic relationship between the replacement chert in the Boone Formation and the ore deposits. It also explores the potential that the silica source for the non-hydrothermal chert is volcanogenic ash, which would have been produced by an island arc associated with Ouachita Orogenic belt. Within the literature, the abundant cherts in the rock record have generally been attributed to silica-secreting organisms, particularly sponge spicules, and the tests of radiolarians, and diatoms (Hesse, 1990). The sheer volume of silica in the Boone Formation and Arkansas Novaculite raises the question of whether organisms could possibly have accounted for all of the silica that comprises those cherts and novaculites, and have at least some preserved. Many other silica sources have been proposed as well, including crustal weathering with river transport, hydrothermal venting, eolian

dust, and altered volcanic ash, among others (Tarr, 1926; Cecil, 2004; Cecil, 2015; Goldstein, 1959).

1.2 Study Location

This study includes samples from exposures in both the tri-state region of northwestern Arkansas, southwestern Missouri, and northeastern Oklahoma, as well as the Ouachita Mountains Region of Arkansas (Figure 1). The Lower Mississippian chert-bearing carbonates in the tri-state area are rather freshly exposed in road cuts, providing readily available stratigraphic sections to sample. Key outcrops of the Boone Formation used in this study are located near Bella Vista, Arkansas (36°24'47.04"N, 94°12'51.18"W); Pineville, Missouri (36°34'2.85"N, 94°21'32.74"W); and Kansas, Oklahoma (36°12'40.32"N, 94°46'16.97"W). Arkansas Novaculite samples were collected from the Caddo Gap exposure (34°23'19.63"N, 93°36'30.67"W) in the Ouachita Mountains. Single samples were collected from intervals both above and below the Boone Formation for comparison. A chert sample was collected from the Pierson Member of the St. Joe Formation (referred to as the Pierson Formation in Missouri) at the Branson Airport exposure (36°32'37.39"N, 93°11'49.63"W). An additional chert sample was collected from the Pitkin Formation (Upper Mississippian) in an exposure along Wolf Creek near Deer, Arkansas (35°51'45.02"N, 93° 8'58.83"W). For additional comparison, two samples of the Hatton Tuff, exposed near Hatton, Arkansas (34°21'3.22"N, 94°22'16.60"W), were collected and analyzed as well. Figure 1 provides sample locations overlain on a map of the major tectonic provinces of the study region. Samples were chosen to reflect a geographic and stratigraphic distribution of the Lower Mississippian siliceous deposits.

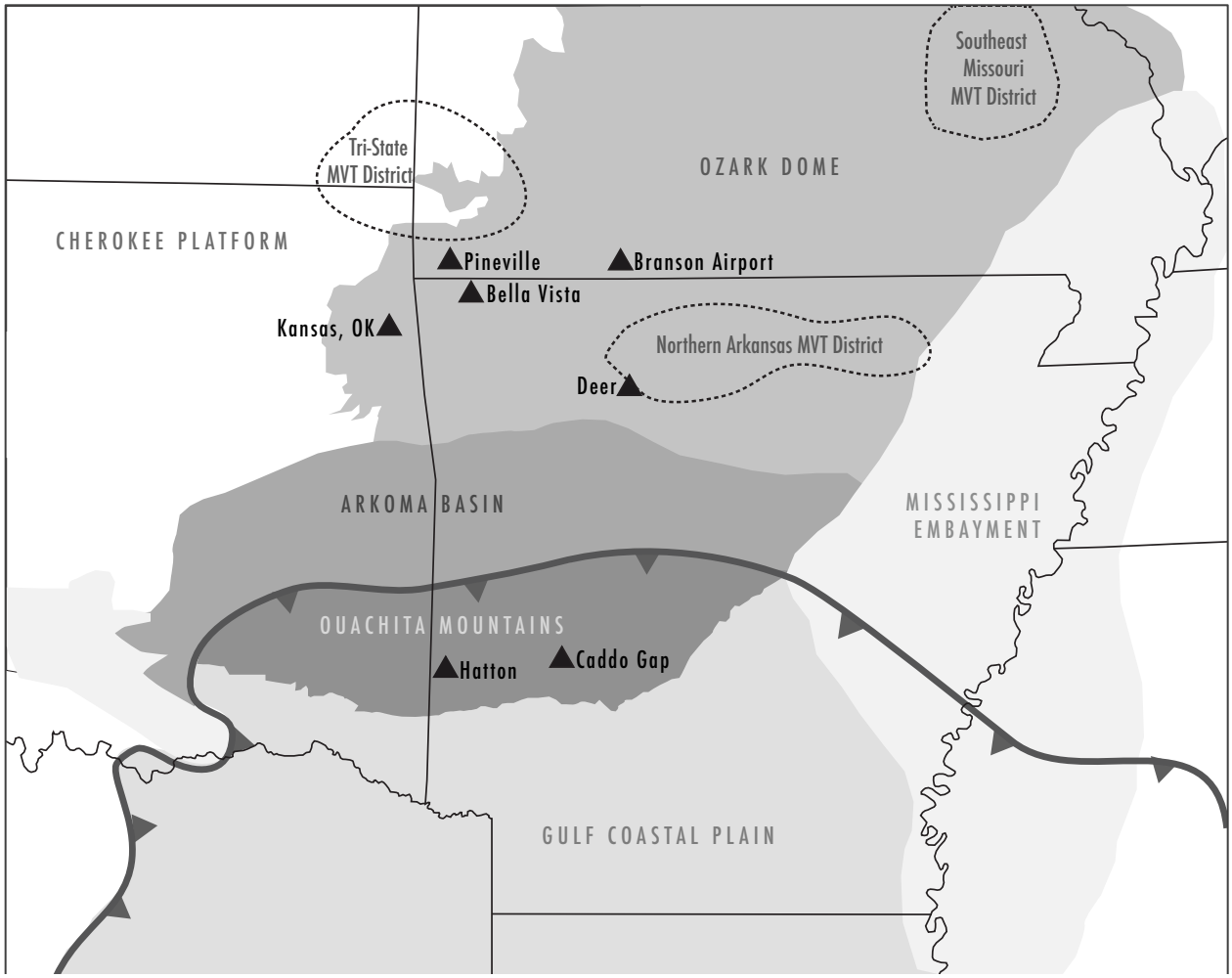

Figure 1. Sample locations overlain on map of tectonic provinces of Arkansas and adjacent areas with Mississippi Valley-Type Ore Districts represented by dashed lines (modified from Manger, Zachry, and Garrigan, 1988; MVT district locations from Bradley and Leach, 2003).

2. GEOLOGIC SETTING

The Southern Midcontinent Region of North America is characterized by a cratonic setting whose stratigraphic record reflects multiple eustatic cycles of transgression and regression by epeiric seas through most of the Paleozoic and Mesozoic Eras. The area including Arkansas, Oklahoma, and Missouri, can be divided into four geographic regions: the Ozark Dome, the Cherokee Platform, the Arkoma Basin, and the Ouachita Mountains (Figure 1).

2.1 Ozark Dome

The Ozark Dome is a broad cratonic uplift cored by Precambrian granite and rhyolite that crops out in southeastern Missouri as the St. Francois Mountains. A sedimentary section comprising Cambrian-Middle Pennsylvanian units dips radially away from the core area, steeper on the east and north flanks, gentler on the south and west flanks. Northeastern Oklahoma and northern Arkansas make up the southern and western flanks of the dome, where beds are regionally dipping less than one degree (Chinn and Konig, 1973). A series of major *en echelon* normal faults, trending northeast-southwest and downthrown on the southeast, are the main structural complications (Hudson, 2000).

Three plateau surfaces develop away from the center of the Ozark Dome as a result of the thickness and resistance to erosion of the sedimentary units as well as the epeirogenic uplifts. These plateau surfaces, in order of oldest to youngest and increasing elevation, are the Salem, Springfield, and Boston Mountains Plateaus. The Salem Plateau is lowest topographically, and exposes Ordovician limestones and dolomites in northern Arkansas, with associated, but more limited, orthoquartzitic sandstones and shale. The Springfield Plateau is capped by the Lower Mississippian limestone and chert of the St. Joe and Boone Formations. The Boston Mountains Plateau is capped by the Lower-Middle Pennsylvanian Atoka Formation, which is the youngest formation in the southern Ozarks.

2.2 Arkoma Basin

The Arkoma Basin is a topographic and structural low that lies between the Ozarks and the Ouachita Mountains, and trends east-west across central Arkansas and south-central Oklahoma. It extends from the Mississippi Embayment on its eastern edge to the Arbuckle Mountains in the west and covers an area of approximately 33,800 square miles. The southern boundary of the basin is traditionally placed at the first persistent thrust faults of the frontal Ouachita Mountains. The Arkoma Basin formed as a foreland basin in response to the compressional tectonics of the Ouachita Orogeny. This south-west-plunging syncline is asymmetrical, with gentle dips on its northern margin and steeper dips on its southern margin. Moving north of the frontal Ouachita thrusts, the area is folded into a series of east-trending, and generally east-plunging, anticlines and synclines (Diggs, 1961). This area of significant folds passes into a more fault-dominated region northward (Diggs, 1961). This faulting is predominantly down-to-the-basin normal faulting with high angle fault planes. The Arkoma Basin is expressed today as a topographic low due to erosion by the Arkansas River, whose valley is controlled by the resistance to weathering of the associated, folded rock units (Guccione, 1993).

2.3 Cherokee Platform

The study area is bounded to the west by the Cherokee Platform. The Cherokee Platform is an area of approximately 26,500 square miles comprising northeastern Oklahoma, southeastern Kansas, and southwestern Missouri. Similar to the Ozark Dome, the Cherokee Platform occupies a cratonic setting that reflects deposition by the transgression and regression of epeiric seas. This results in a geologic record characterized by thin sedimentary units with frequent regional facies changes and numerous unconformities. As in Northern Arkansas, the

Lower Mississippian carbonate successions are composed of material produced on the Burlington Shelf, which was then transported down ramp and deposited.

2.4 Ouachita Mountains

The Ouachita Mountains are a broad anticlinorium comprised of folded and faulted Paleozoic strata, deformed by compressional tectonics associated with plate collision between Laurasia and Gondwana during the Carboniferous. The deformed belt of Paleozoic rocks that comprises the Ouachita system (Figure 2) extends from east-central Mississippi westward and southward along a sinuous course into Mexico (Flawn, 1961). The Ouachita Mountains of eastern Oklahoma and western and central Arkansas are the largest area of exposure of the deformed belt, which is concealed for approximately 80 percent of its total length (Flawn, 1961). The complexity of the folding of Paleozoic strata comprising the Ouachita Mountains makes it difficult to measure true stratigraphic thickness.

Figure 2. Paleozoic basins in the southeastern United States (modified from Harry and Mickus, 1998).

2.5 Tectonic Evolution

The tectonic evolution of the region began with initial rifting of Rodinia in the earliest Paleozoic as Laurasia separated from Gondwana (Figure 3; Houseknecht and Matthews, 1985). From the earliest Paleozoic to earliest Mississippian time, the region was characterized by a stable passive margin phase in which deposition of thin stratigraphic units occurred along the Northern Arkansas Structural Platform, which was positioned along the southern margin of Laurasia. During the Carboniferous Period, the tectonic regime evolved from a stable passive margin to a foreland basin phase. Sedimentation rate and volume increased dramatically in the middle Atoka, reflecting subsidence and increase in accommodation resulting from flexural down-warping caused by the convergence of a continental landmass to the south. This collisional event and development of a subduction zone led to the formation of the Arkoma foreland basin in the middle Atokan. As convergence continued, the Ouachita Mountains were formed as an accretionary prism as the sedimentary units previously deposited in the Ouachita Trough were folded and thrusted (McGilvery et al., 2016). Post-orogeny, Triassic-Jurassic rifting led to the breakup of Pangea as South America broke away from the southern part of North America, resulting in the formation of the Atlantic Ocean and the Gulf of Mexico (Guccione, 1993).

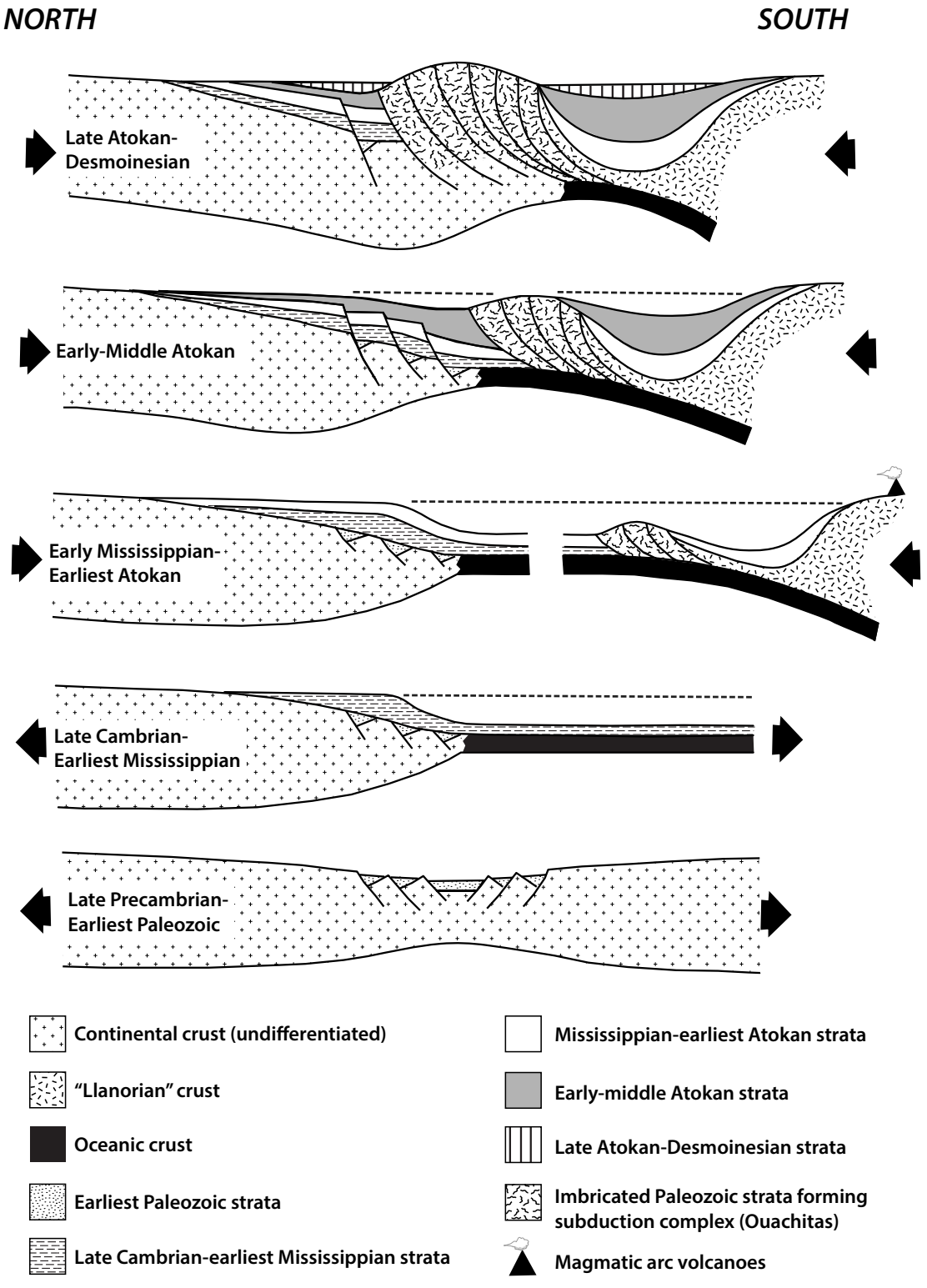

Figure 3. Cross sections depicting the tectonic evolution of the southern margin of North America. Modified from Houseknecht and Matthews (1985).

2.6 Mississippian Paleogeography

During the Lower Mississippian, the southern midcontinent was a broad, shallow, carbonate platform designated the Burlington Shelf (Lane, 1978; Lane and DeKeyser, 1980; Gutschick and Sandberg, 1983) (Figure 4). This shelf acted as a carbonate factory, producing abundant carbonate mud and crinozoan and other bioclastic detritus, with excess material being transported down-ramp and deposited across northern Arkansas and northeastern Oklahoma by gravity-driven processes. An isopachous map of the St. Joe Limestone in northern Arkansas displays a lobate pattern produced by down-ramp sediment transport (Handford and Manger, 1990). The carbonates of the St. Joe and Boone interval represent similar depositional conditions on a shallow ramp, but reflect changes in sea level as the seas transgressed and regressed during the Lower Mississippian.

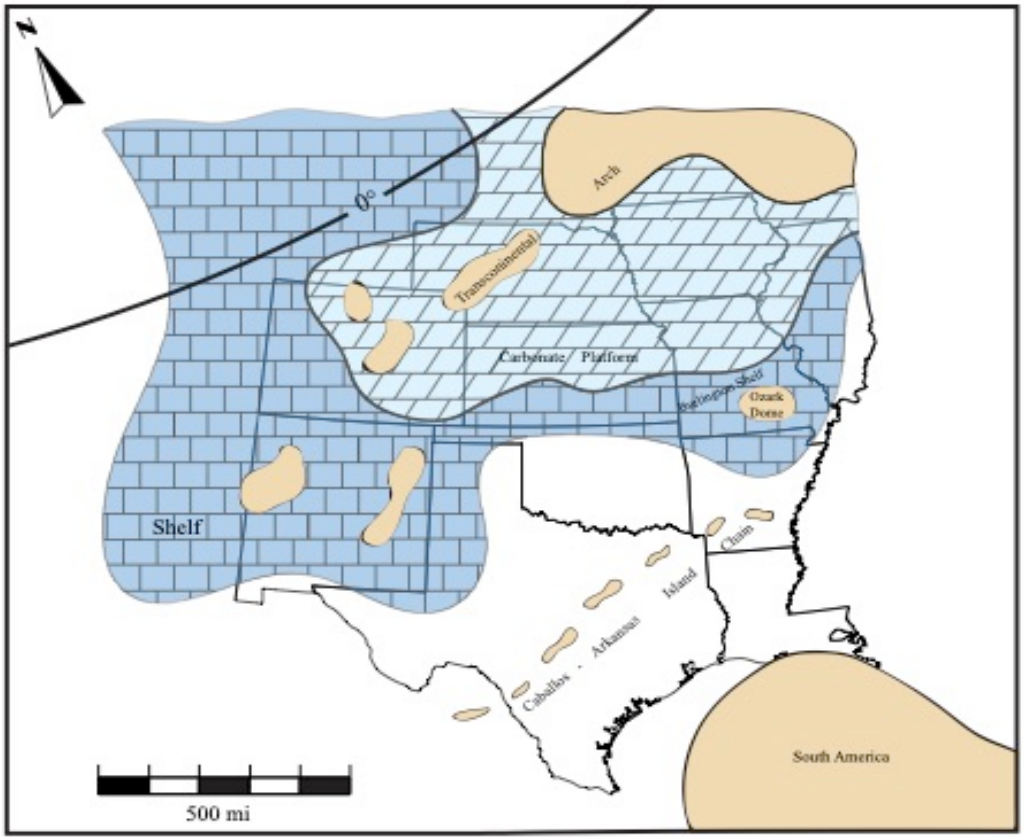

Figure 4. Lower Mississippian paleogeography illustrating the distribution of lithofacies across the southern midcontinent region. Figure from McFarlin (2018) after Gutschick and Sandberg (1983).

3. STRATIGRAPHIC FRAMEWORK

3.1 Overview

This study primarily focuses on siliceous rocks of the Boone Formation and the Arkansas Novaculite, but also includes limited sampling from the St. Joe, Hatton Tuff, and Pitkin Formation. The Boone Formation is entirely Lower Mississippian, while the Arkansas Novaculite is considered to be Devonian-Mississippian, with the informal upper Novaculite representing the stratigraphic equivalent to the Boone Formation. Figure 5 shows the general stratigraphic relationship between all the samples analyzed in this study.

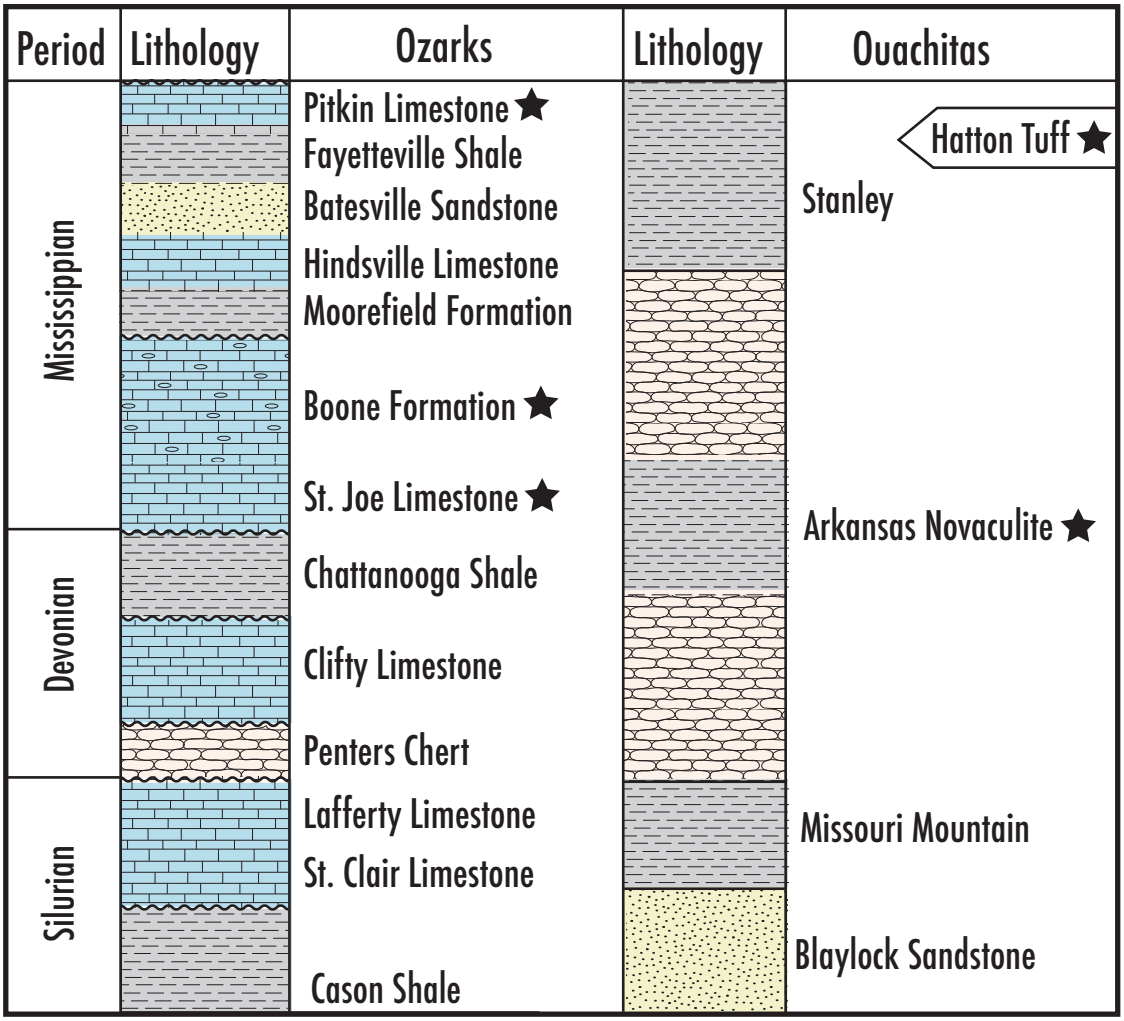

Figure 5. Generalized stratigraphic column showing approximate stratigraphic relationship of sampled intervals in this study, indicated by stars. No relative thickness is implied by these charts. (modified from MacFarland, 1998).

3.2 St. Joe and Boone Formations

The Lower Mississippian St. Joe and Boone Formations represent a single, third-order, transgressive-regressive, unconformity-bounded eustatic cycle (Figure 6). The transgressive systems tract is represented by the St. Joe Limestone, which is mostly chert-free, although penecontemporaneous chert is found occasionally at several localities. Overlying the St. Joe, the Boone Formation is informally divided into lower and upper members based on lithology and chert development in response to maximum flooding, highstand and regression (Figure 6). The lower Boone represents the maximum flooding interval of a third-order cycle producing calcisiltites and dark, nodular, penecontemporaneous chert. The upper Boone represents the highstand and regressive systems tract and comprises coarse, crinoidal limestones alternating with thin, carbonate mud-supported lithologies and replacement by later diagenetic chert. The interval is bounded by an unconformity at its top (Figure 6).

In this region, several changes in stratigraphic nomenclature ("Stateline Faults") occur crossing state lines. The names applied as members of the St. Joe in Arkansas are considered formations in southwestern Missouri (Bachelor, Compton, Northview, and Pierson - ascending order). The stratigraphic equivalent of the lower Boone in northern Arkansas is the Reeds Spring Formation in Missouri and Oklahoma. The upper Boone is divided into multiple units as it extends northward into Missouri, with the lower part of the interval designated the Elsey Formation, and the upper part as the Burlington-Keokuk undifferentiated. The Burlington and Keokuk are treated as differentiated formations northward in Iowa, where their respective type localities are located.

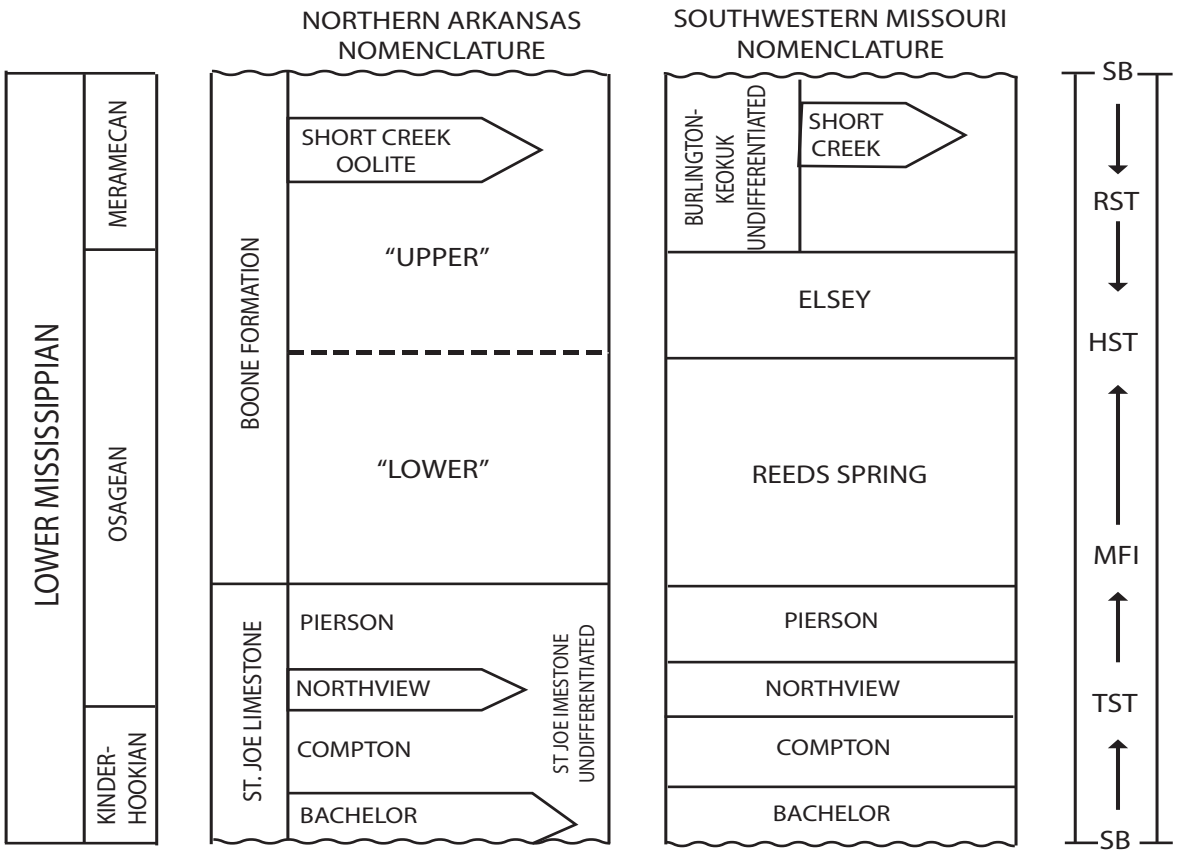

Figure 6. Stratigraphic column representing Lower Mississippian strata in northern Arkansas and equivalent units in southern Missouri. (Modified from Manger and Thompson, 1982).

3.3 Arkansas Novaculite

The Arkansas Novaculite was named by Griswold (1892), and later divided into three members (Miser, 1917; Lowe, 1989) based on lithology: a lower novaculite member, a middle member of interbedded chert and shale, and an upper novaculite member. Lithologically, the term novaculite has been applied somewhat inconsistently. Miser and Purdue (1929) described it as "a gritty, fine-grained, homogenous, highly siliceous rock, possessing a conchoidal or subconchoidal fracture and being translucent on thin edges." Later, Sholes and McBride (1975) described the novaculite as consisting of polyhedral grains of microcrystalline quartz ranging in size from 5 to 20 microns across. These descriptions of the lithologic character are consistent with exposures of the Arkansas Novaculite, which crops out along the flanks of the Benton Uplift of the Ouachita Mountains. The white siliceous rocks were initially designated

lithologically as novaculite, but later, the name became a lithostratigraphic term that described the entire siliceous interval, which is underlain and overlain by sandstones, shales, and limestones (Park, 1961).

The age of the Novaculite is poorly constrained, but the middle member of the Arkansas Novaculite has been shown, using conodonts, to cross the Devonian-Mississippian boundary (Park, 1961). The lower Novaculite is undated, but it overlies the Missouri Mountain Formation, which unconformably overlies the Blaylock Sandstone, which contains a lower Silurian graptolite assemblage (Wilson and Majewske, 1960; Park, 1961).

The Stanley Formation overlies the Arkansas Novaculite and is composed of shale with interbedded sandstone. The Stanley also contains minor amounts of chert as well as five major tuff sequences (Niem, 1971), including the Hatton Tuff, which was sampled for this study. Niem (1977) described the Hatton Tuff as ranging in thickness from 7-40 m consisting of varying proportions of ash-sized, embayed, quartz crystals, plagioclase crystals, relict shards, volcanic dust, and altered pumice fragments. Niem (1977) suggested a southern volcanic source for the tuff sequences that may have been part of a magmatic arc formed by the convergence between the North American plate and a southern continental plate during the Devonian-Mississippian interval.

4. BOONE CHERT DEVELOPMENT

4.1 Overview

Three types of chert development have been recognized and described within the Lower Mississippian succession in northern Arkansas: penecontemporaneous, later diagenetic, and tripolitic chert (Shelby, 1986; Minor, 2013; Cains et al., 2016; McKim, 2017; McFarlin, 2018). Each chert type can be easily differentiated in hand sample and outcrop and reflects changes in depositional environment and the lithology of the limestone.

4.2 Penecontemporaneous Chert

The Lower Boone carbonate mudstones and calcisiltites contain dark, nodular, typically unfossiliferous chert (Figure 7). This chert disrupts the bedding of the limestone and exhibits compaction features, indicating deposition prior to lithification of the limestone, hence its designation as penecontemporanous chert. This chert is associated with deeper water settings, forming as amorphous opaline silica and undergoing the diagenetic transformation to cryptocrystalline quartz. Studies on deep-sea sediments have supported the mineralogical transformation of siliceous sediments through the following diagenetic maturation sequence: opal-A (siliceous ooze) → opal-CT (porcelanite) → chalcedony (micro-fibrous quartz) → cryptocrystalline quartz (chert) (Kastner et al., 1977). This transformation involves a solution-redeposition mechanism, controlled by factors such as temperature, time, composition of the solution, and composition of the host sediments. Kastner and others (1977) showed through experimentation that this transformation rate is higher in carbonate sediments than in clay-rich sediments. The presence of pervasive shrinkage fractures within the lower Boone chert is evidence of water being expelled from the crystalline structure of opaline silica during the mineralogical transformation (Figure 8).

Figure 7. Lower Boone penecontemporaneous chert and limestone in a roadcut along Highway 412 near Hindsville, Arkansas. Photo by author.

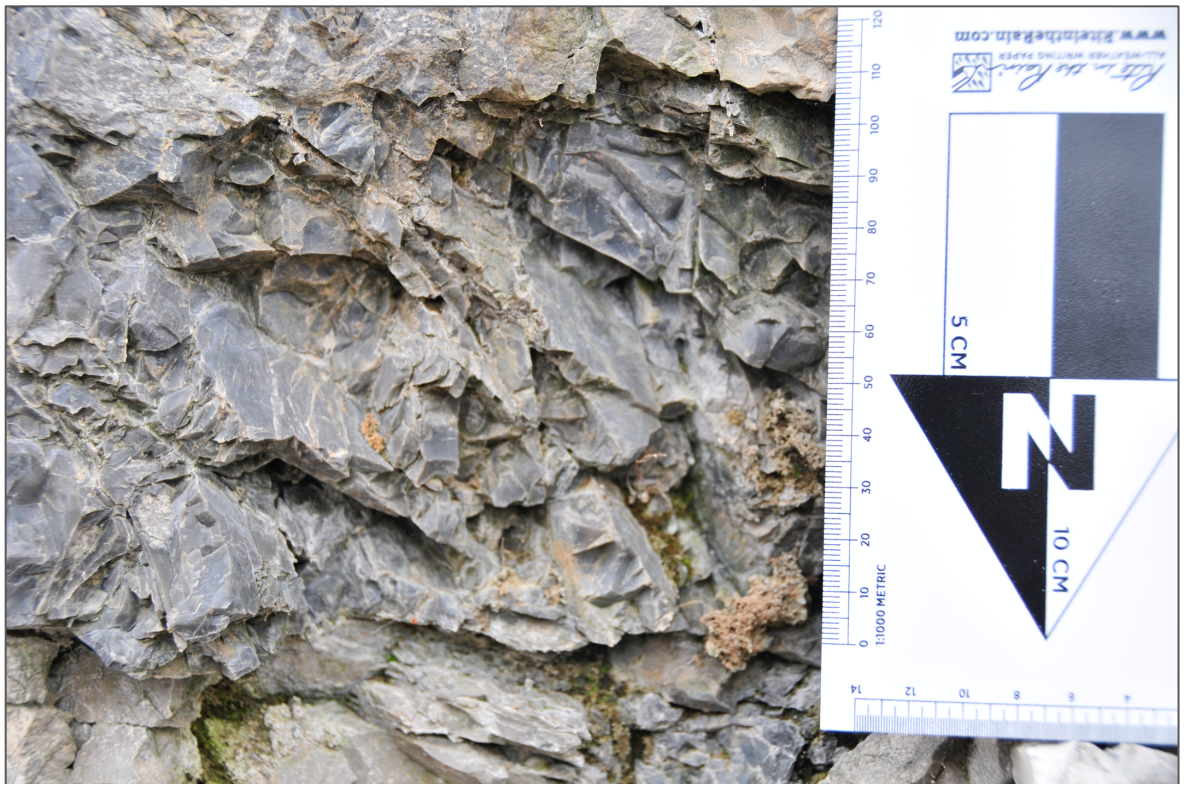

Figure 8. Shrinkage fractures in lower Boone chert. Photo by author.

4.3 Later Diagenetic Chert

The upper Boone contains a white replacement chert that has selectively replaced the finer grained carbonate intervals along bedding planes, and has been designated as later diagenetic chert (Shelby, 1986; Minor, 2013; Cains et al., 2016; McKim, 2017; McFarlin, 2018). This chert is typically white, bedded, and fossiliferous, and replicates the fabric of the limestone being replaced (Figure 9). Thin sections show obvious replacement fabrics within this chert. Replacement is often incomplete, with larger unaltered, usually bioclastic grains being surrounded by chert. The later diagenetic chert is restricted to the upper Boone interval, and was likely emplaced by groundwater. Knauth (1979) proposed a groundwater model for the replacement of limestone by silica that suggests a mixing zone at the contact between meteoric water and sea level. The replacement must have occurred prior to Chesterian deposition because there are later diagenetic chert clasts in a basal breccia in the Hindsville Formation (Figure 10).

Figure 9. Bella Vista outcrop of upper Boone Formation. Interval above the green line is limestone (dark gray) containing later diagenetic chert (white bands). Below the green line is the tripolitized chert interval. Note the distinct difference in weathering character between the chert above and below the green line. Photo by author.

Figure 10. Chert breccia in basal Hindsville Limestone, overlying the upper Boone Formation near Goshen, Arkansas. Photo by author.

4.4 Tripolitic Chert

In some areas, the basal part of the upper Boone contains tripolitic chert, which is a porous-textured, white replacement chert. This chert is interpreted as a hydrothermal replacement of limestone by silica to form the fine-grained, even-textured, white chert, which was later tripolitized as the remaining disseminated carbonate within the chert was removed by groundwater. The dissolution of remaining carbonate within the replacement chert is essential for the formation of tripolitic chert, according to Tarr (1926). A later pulse of hydrothermal fluid passed through the interval precipitating terminated and doubly terminated quartz crystals within the pore spaces of the tripolitic chert (McKim et al., 2017). The tripolitic chert varies significantly from the later diagenetic chert in that it does not follow bedding planes, but rather occupies thick intervals above the lower Boone, and mechanically weathers easily and falls away from exposed outcrop surfaces due to its porous nature (Figure 11). In outcrop, the tripolitic

chert appears as massive, white, very fine-grained chert with remnant, pseudo-nodular limestone bodies.

Figure 11. Tripolitic chert outcrop along I-19, near Anderson, Missouri. Note crumbling nature of porous tripolitic chert at foot of outcrop. Photo by author.

5. MISSISSIPPI VALLEY-TYPE ORE DEPOSITS

5.1 General Characteristics

Mississippi Valley-Type (MVT) lead-zinc ore deposits are found worldwide. The largest MVT deposits are found in North America, and these deposits are named for several well-known districts in the Mississippi River drainage basin of the United States (Leach et al., 2010). MVT ore deposits are characteristically hosted by carbonate sequences of either dolostone or limestone. They typically occur at the flanks of basins or within foreland thrust belts. These deposits are unrelated to igneous rock emplacement, but rather are emplaced by ore-bearing fluids derived from evaporated seawater and then driven through carbonate rocks by tectonic events (Leach et al., 2010). Bradley and Leach cite the definition of MVT lead-zinc deposits as "a varied family of epigenetic ores precipitated from dense basinal brines at temperatures ranging between 75 and 200°C, typically located in platform carbonate sequences and lacking genetic affinities to igneous activity" (Bradley and Leach 2003, Leach and Sangster 1993).

5.2 Ore Districts of the Southern Ozarks Region

The Southern Ozarks Region includes the Tri-State Mining District and the Northern Arkansas District (Figure 1). The Tri-State district is located across northeast Oklahoma, southwest Missouri, and southeast Kansas. The ore deposits in the Northern Arkansas district are primarily emplaced within Ordovician dolomites and Mississippian carbonates (Figure 12)., while in the Tri-State District, they are primarily emplaced within the Mississippian Boone Formation (Figure 12).

In most MVT deposits, silicification is generally minor, but it is well developed in the Tri-State and Northern Arkansas districts (Brockie et al., 1968; McKnight, 1935). The Ozark Region is one of many regions where the fluid inclusion temperatures exceed the expected thermal gradient and stratigraphic burial temperatures (Leach et al., 2010). With the

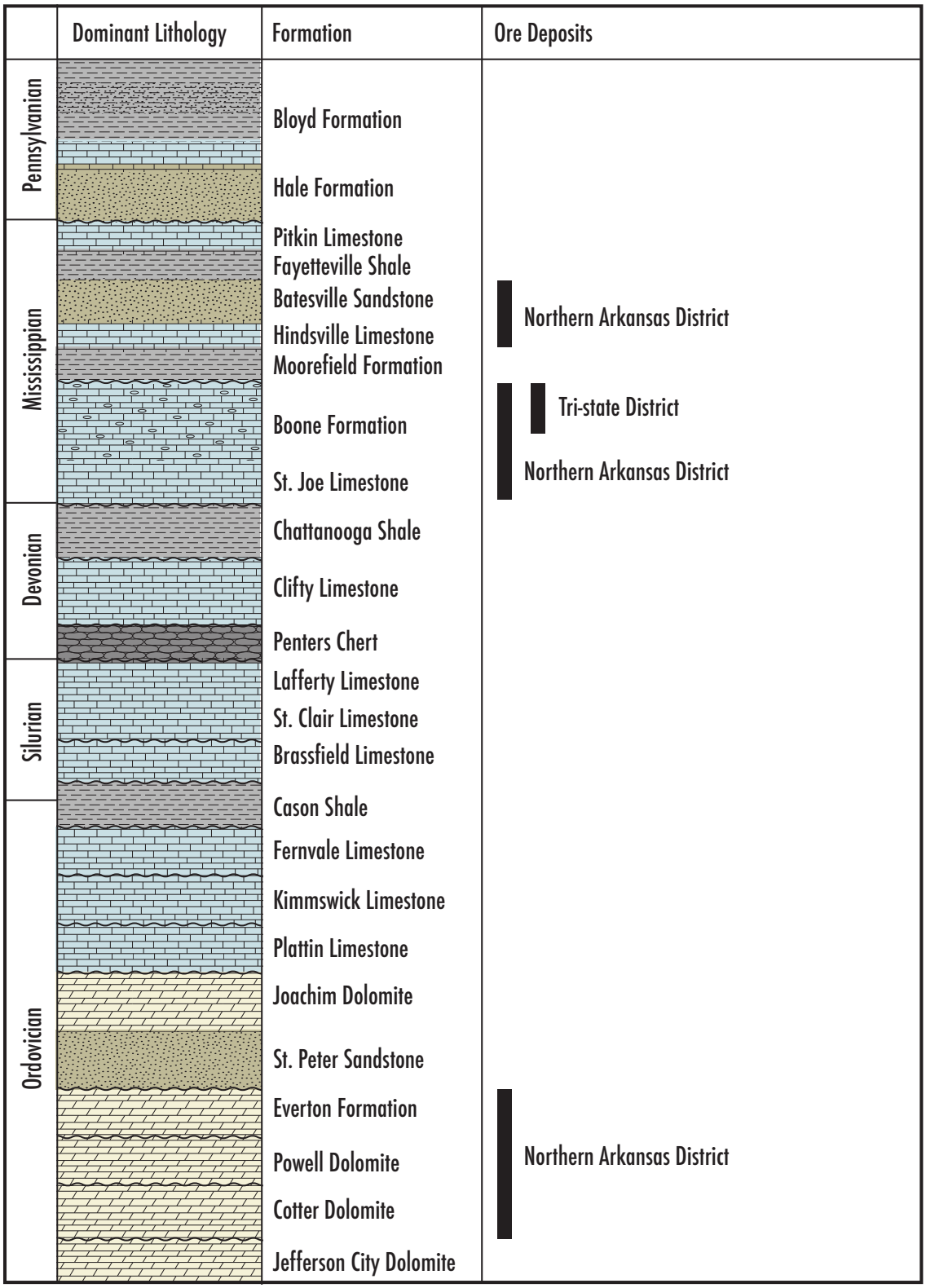

Figure 12. Generalized stratigraphic column of the southern Ozark region in northern Arkansas showing the approximate stratigraphic position of Mississippi Valley-type ore deposits. Modified from Wenz et al. (2012) and Liner et al. (2013).

Ozark MVT deposits, the temperatures are explained by unusually high geothermal gradients, advection from the deeper basin, and/or ascent of deeply circulating fluids in the basement (Leach et al., 2010). The ore fluid composition measured from fluid inclusions in the sphalerite ores are similar to present-day brines formed from subaerially evaporated seawater (Kesler et al., 1996; Viets and others, 1996; Leach et al., 2005). The MVT deposits in the Midcontinent region of the United States contain very radiogenic Pb, which indicates either a basement source or sedimentary rocks derived from the basement (Leach et al., 2010).

5.3 Tectonic Controls

Many authors have recognized that MVT deposits are related to orogenic forelands both temporally and spatially (Leach et al., 2010). The majority of dated MVT Pb and Zn deposits coincide with the formation of Pangea during the Devonian through Permian. Bradley and Leach (2003) provide a rather concise description of the series of events potentially leading to the mineralization in the Ozark Region that follows. The host carbonates were deposited along the passive margin initially. Subduction began in the ocean basin, leading to convergence of the incoming arc and passive margin; flexure of the passive margin drove subsidence of the foredeep and also caused extensional faults, which may later have focused fluid migration. After collision between Gondwana and Laurasia, the foreland basin filled with siliciclastic sediments. Uplift of the mountains and proximal foreland basin due to erosional unloading provided the topographic relief necessary to drive MVT fluids toward the adjacent foreland (Bradley and Leach, 2003). Syn-collisional normal faults in the Ouachita foreland localized mineralization producing the Northern Arkansas MVT district (Bradley and Leach 2003).

Figure 13 represents Permian conditions, when the ore deposits were emplaced, and shows the relative position of the Northern Arkansas, Tri-State, Southeast Missouri, and Central Missouri MVT districts. The MVT deposits are younger in the south (Northern Arkansas is

265±20 Ma; Leach, 2001) than in the north (Central Missouri is 303±17 Ma; Leach, 2001), which may be attributed to forebulge migration toward the orogen (Bradley and Leach, 2003) (Figure 13).

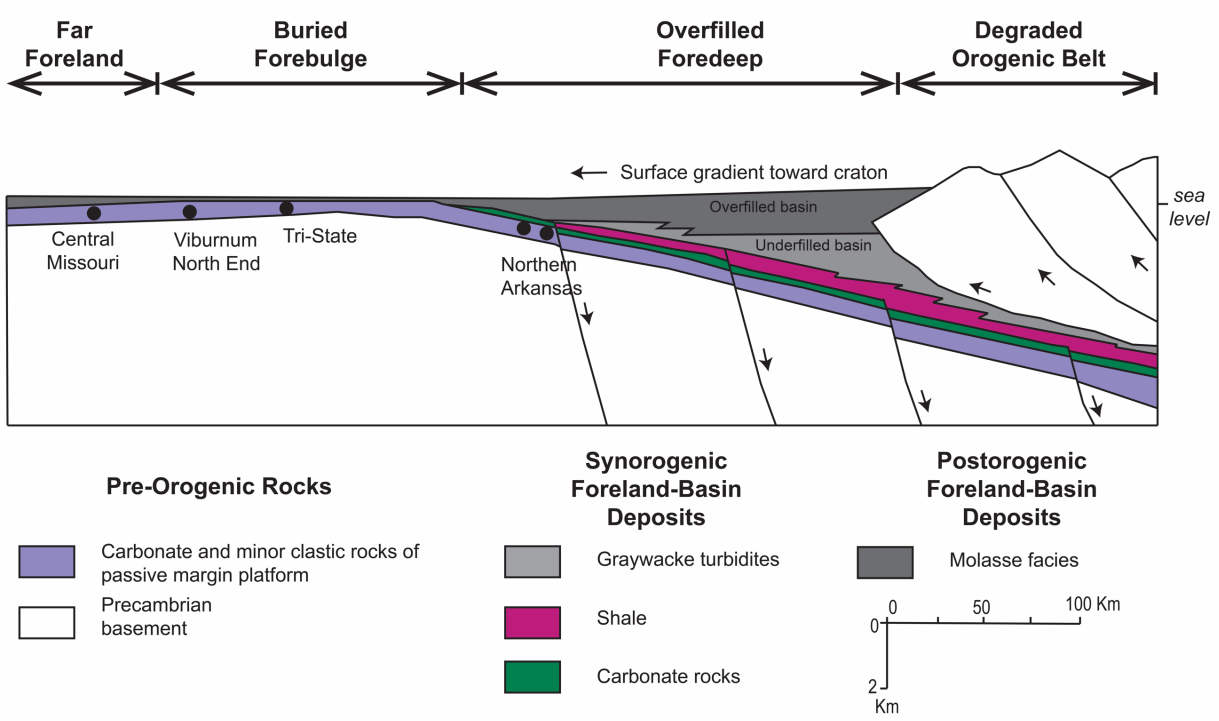

Figure 13. Schematic north-south cross section through the Ouachita orogen and its foreland, representing conditions in Permian time, after plate convergence and emplacement of the MVT deposits had ended (modified by John Samuelsen from Bradley and Leach, 2003).

6. PREVIOUS INVESTIGATIONS

Several geochemical studies have been conducted over the last several years that contribute to the current understanding of the MVT ores and are applicable to the Boone Formation cherts, and the Arkansas Novaculite. Potra et al. (2018) used Pb isotope trends to identify potential source regions for the MVT deposits in the Northern Arkansas district, the Tri-State district, and the Burkesville deposit in the Central Kentucky district. The Northern Arkansas ores show a linear trend of isotopic ratios, suggesting mixing between two components. Potra et al. (2018) analyzed Chattanooga Shale samples, which plotted close to the non-radiogenic end of the Northern Arkansas ores, suggesting they may be the non-radiogenic end member source of Pb for those ores.

Bottoms et al. (2019) analyzed ores from the Northern Arkansas and Tri-State Mining districts as well as shale samples from the Chattanooga Shale and Fayetteville Shale. The ores in both districts are enriched in radiogenic isotopes, and the districts exhibit overlapping signatures, suggesting they may share a common source. Bottoms et al. (2019) proposed an alternative model that organic-rich shales may be the only source of metals for the ores. This model suggests that organic molecules progressively release adsorbed metals as they mature and crack.

Chick et al. (2017) proposed a hydrothermal origin for the tripolitic chert and its potential relationship to the Tri-State Ore district. This hydrothermal event must have included multiple pulses of hydrothermal fluid movement. Early on, the carbonate of the upper Boone was replaced by silica, likely by the movement of silica-bearing hydrothermal fluids. During emplacement, those fluids are interpreted as confined between the layers of penecontemporaneous chert and limestone of the lower Boone and the later diagenetic chert and limestone layers of the Elsey/upper Boone, thus, acting like a confined aquifer (McKim, 2017). After silicification, the remaining disseminated carbonate within the interval that had experienced replacement was

leached out, likely by groundwater invasion (Chick et al., 2017). This leaching produced the porous texture that is characteristic of the tripolitic chert interval (Figure 18). Terminated and doubly terminated quartz crystals crystallized within the pore spaces of the tripolitic chert, photographed by Minor (2013) and McKim (2018) using Scanning Electron Microscopy (Figure 14). These terminated quartz crystals were likely emplaced by a later pulse of hydrothermal fluid movement, occurring after the chert had been leached to create void spaces (Chick et al., 2017).

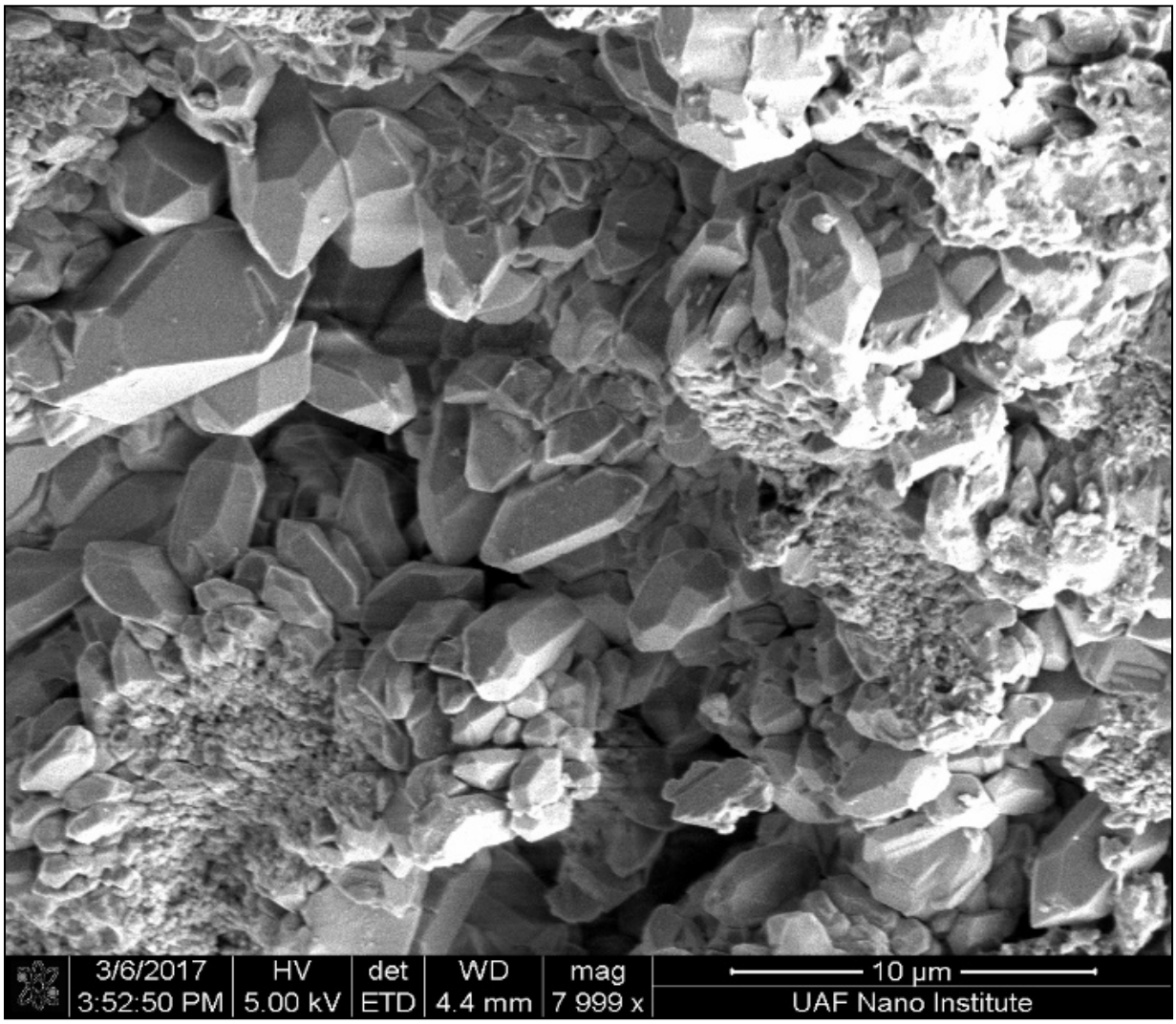

Figure 14. Terminated and doubly-terminated quartz crystals in the upper Boone tripolitic chert. Image by McKim (2018).

Several studies have also been conducted which investigate the silica source of the Arkansas Novaculite and the Boone cherts. Philbrick (2016) and Cains et al. (2016) looked at

trace element concentrations in the Arkansas Novaculite and the Boone, respectively, and concluded that they showed similar elemental concentrations consistent with those of average magmatic arcs, suggesting a relationship between the chert and an arc source. Similar concentrations between the Boone penecontemporaneous cherts and the Arkansas Novaculite also suggest that they formed from the same volcanic source (Philbrick, 2016). Energy dispersive x-ray data showed concentrations of both aluminum and potassium, which would seem to favor a volcanic silica source over a biogenic one (Philbrick, 2016).

7. METHODS

7.1 Sample Collection

Whole rock samples were collected from several localities in the southern midcontinent (see Figure 1 and Appendix for detailed sample locations). The sampling strategy was to collect both a stratigraphic and geographic distribution of samples. The primary focus of this study is to evaluate the mode of formation and silica source for the Mississippian Boone chert, and to determine whether there is a geochemical similarity to the Devonian/Mississippian Arkansas Novaculite. While it is necessary to acknowledge that only the upper member of the Novaculite is stratigraphically equivalent to the Boone Formation, for comparison, the lower Novaculite was also analyzed. Additionally, single samples from above and below the Boone Formation were analyzed, one each from the St. Joe and Pitkin Formations, respectively. The final two samples analyzed were Hatton Tuff samples from Hatton, Arkansas. The Hatton Tuff is of Mississippian age, and a member of the Stanley Formation. It is interpreted to be a submarine ash flow, providing a comparison with rocks of known igneous origin in the area. Photographs were taken of each sample prior to analysis (Figure 15).

Figure 15. Slab samples from lower Boone (left) and upper Boone (right).

7.2 Sample Powdering

Each hand sample collected from outcrop was prepared by cutting one-centimeter thick slabs of rock. Three cuts were made to self-contaminate the saw, and the final slab was collected for use. Each slab was rinsed in deionized water and allowed to dry. Then, each sample was wrapped in aluminum foil, paper towel, and plastic, and broken to retrieve the freshest, most uncontaminated pieces of the slabbed rock. These chips were then powdered using a Spex SamplePrep Shatterbox, which uses a ceramic alumina container to crush the rock (Figure 16). This container was self-contaminated by powdering and discarding the first two sets of chips. The third and final set of chips was powdered and collected in polypropylene cups, previously leached in hot HNO_3. Between each sample, the ceramic alumina container was cleaned with deionized water and allowed to dry. Previously HNO_3-leached quartz sand was powdered between samples to prevent cross contamination, and the ceramic alumina container was cleaned again with deionized water and double distilled water, and allowed to dry.

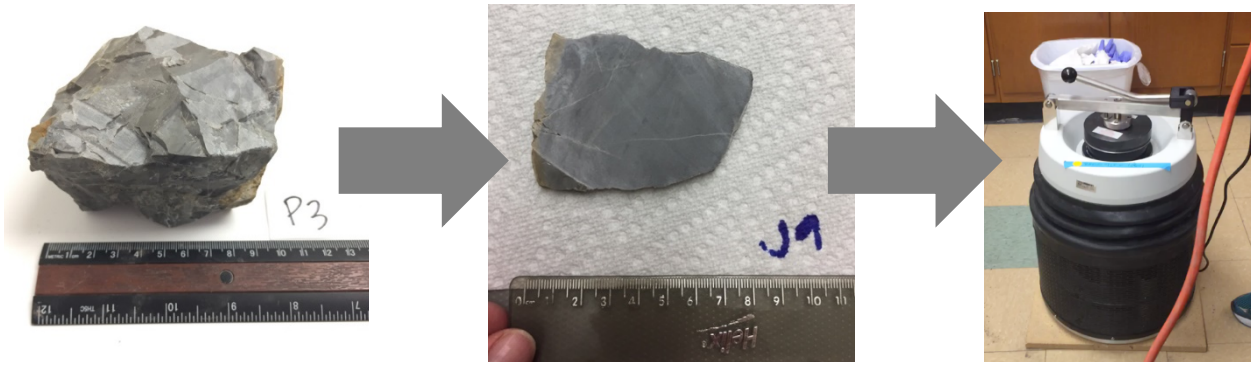

Figure 16. Hand sample, sample slab, and shatterbox used to powder samples.

7.3 Sample Processing for Trace Element Concentration Analysis

For trace element concentration analysis, 32 samples, six USGS rock standards, one duplicate, and one blank were processed. For silicate dissolution, around 150 mg of each sample powder (accurate weight recorded for each sample) was weighed in Teflon Savillex capsules

Three mL of 7N HNO_3 and 2 mL of concentrated HF were added to each sample powder and the capsules, with lids on, were placed on the hot plate at 170°C for 8 hours in order to digest the sample powder. Following this step, the sample solution was dried at 150°C. One mL of 6N HCl and 1 mL of 7N HNO_3 were added to the dried sample and the capsules were placed on the hot plate at 200°C until the samples were redissolved. One Boone chert and two Arkansas novaculite samples retained some undissolved particles. Hydrogen peroxide was added to all three samples and the Boone sample reacted immediately, indicating the presence of organics. The novaculite samples J35 and J36 experienced a delayed reaction to the H_2O_2; however, they did eventually lightly effervesce. All samples were dried at 100°C. Two mL of concentrated HNO_3 were added and the samples were heated again at 200°C until dissolved and then dried at 100°C. Two mL of 7N HNO_3 were added to redissolve each sample. At this stage, the samples were digested and ready to be analyzed for trace element concentration on a Thermo Scientific iCAP Q ICP-MS. In order to avoid overvolting the detectors, the samples to be analyzed were diluted by a factor of 25. Therefore, 0.2 mL of sample solution was transferred to centrifuge tubes and 4.8 mL of triple distilled water were added to make a 2% HNO_3. In order to build calibration curves and constrain the accuracy and reproducibility of the measurements, six USGS rock standards (AG-2, BHVO-2; BIR-1; DNC-1; QLO-1; W-2) were measured along with the samples. The U, Th, and Pb concentrations allow age-correction calculations to be carried out on the whole-rock samples.

7.4 X-ray Diffraction

X-ray diffraction data were collected from five samples for mineralogical analyses. These samples included one penecontemporaneous Boone chert sample, two Arkansas novaculite samples, and two Hatton tuff samples. Powdered whole rock samples were analyzed using the Philips PW1830 Double System Diffractometer at the Institute for Nanoscience and Engineering, University of Arkansas.

7.5 Sample Processing for Radiogenic Isotope Analyses

Thirty-six samples were processed for Pb, Sr, and Nd isotope analyses, including two blanks and one duplicate. For isotopic analysis, around 300 mg of sample powder were digested similarly to the methods described for trace element concentration analysis. Six mL of 7 N HNO_3 and 4 mL of concentrated HF were added to each sample, which were then placed on the hot plate at 200°C for about 12 hours. The samples were dried at 110°C. Following this step, 1 mL of 6N HCl and 1 mL of 7N HNO_3 were added, and the capsules were placed on the hot plate at 200°C until the samples were dissolved. The caps were then removed, and the samples were dried at 110°C. Two mL of concentrated HNO_3 were added and the samples were heated at 200°C until dissolved, and then dried at 110°C. At this point, 1.5 mL of 1 N HNO_3 were added and the samples were placed on the hot plate at 200°C to redissolve them. The samples were allowed to cool and then transferred to centrifuge tubes. Each sample was centrifuged for 10 minutes, rotated 180°, and centrifuged again for 10 minutes to separate any undigested residue from the digested sample to be used for column chemistry.

Separation of Pb, Sr, and Nd was completed by column chemistry following the methods outlined in Pin et al. (2014). Table 1 outlines the steps involved in column pre-cleaning, sample loading, and elution of Pb, Sr, and Nd. Column procedures involved the use of three resins: Sr spec, TRU spec, and Ln spec. The column pre-cleaning process required the addition of varying volumes of varying concentrations of HCl, HNO_3, and HF, depending on the resin (Table 1). Following pre-conditioning, the samples were loaded in the columns containing the Sr spec resin, with the Sr spec and the TRU spec columns in tandem. The Sr and Pb fractions were eluted with the upper Sr spec columns, and the rare earth elements (REE) were extracted with the lower TRU spec columns. The REE were separated using the TRU spec and the Ln spec columns in

tandem, with the Nd fraction eluted through the Ln Spec columns using sequential addition of 0.25 N HCl (Table 1; Pin et al., 2014).

After column separation, the samples were analyzed for Pb, Sr, and Nd isotope ratios using a Nu Plasma MC-ICP-MS at the University of Arkansas. The Pb samples were dissolved in 2% HNO_3 and diluted based on the Pb concentration of each sample. Thallium (Tl) was added to each sample immediately before analysis to allow the mass spectrometer to correct for internal mass fractionation, making a final solution of approximately 12 ppb Tl. Thallium addition is necessary since Pb does not have two stable isotopes to use for this correction, unlike Sr and Nd. The Pb isotope ratios represent an average of 60 measurements, and each average is corrected for instrumental differences using the NBS 981 Pb standard. See Appendix for Pb standard analyses. The Sr and Nd samples were diluted with 2% HNO_3 and analyzed on the same mass spectrometer. Each ratio represents the average of 50 measurements taken of each sample. The data were corrected for instrumental fractionation based on the analyses of the Sr and Nd standards, NBS 987 (Sr standard) and JNdi (Nd standard).

Table 1. Summary of steps in column separation procedure (Pin et al. 2014).

Column Separation	
Column pre-cleaning and pre-conditioning	
Sr Spec (~250 µL)	Add 3mL 6 N HCl (3x)
	Add 3 mL 0.05 N HNO_3 (3x)
	Add 0.1 mL 1 N HNO_3
TRU Spec (~250µL)	Add 4 mL 0.1 N HCl – 0.29 N HF
	Add 10 mL 0.05 N HNO_3
	Add 0.1 mL 1 N HNO_3
Ln Spec (~800 µL)	Add 3mL 6 N HCl (3x)
	Add 2 mL 0.25 N HCl (2x)
	Add 0.1 mL 0.05 N HCl
Sr Spec and TRU Spec columns in tandem	
Sample loading	1.5 mL 1 N HNO_3
Sample wash	0.5 mL 1 N HNO_3 (x2)
Column decoupling and further elution	
Sr Spec	
Elution of Ba	Add 1 mL 7 N HNO_3 (x2)
	Add 0.5 mL 2 N HNO_3
Elution of Sr	Add 1 mL 0.05 N HNO_3 (x2)
	Add 1 mL 3 N HCl (2x)
Elution of Pb	Add 1mL 6 N HCl (2x)
TRU Spec	Add 1 mL 1 N HNO_3 (2x)
	Add 0.1 mL 0.05 N HNO_3
	Add 0.1 mL 0.05 HCl
Tru Spec and Ln Spec columns in tandem	
LREE back-extraction/loading	Add 0.5 mL 0.05 N HCl (3x)
Column decoupling and further elution	
Ln Spec	
	Add 0.1 mL 0.05 N HCl (2x)
Elution La-Ce-Pr	Add 2.7 mL 0.25 N HCl
Elution Nd	Add 2 mL 0.25 N HCl
Elution Sm	Add 1.5 mL 0.75 N HCl

8. RESULTS

8.1 Trace Elements

Trace element patterns and a comparison of chert types is illustrated by multielement (spider) diagrams, which display relative depletion or enrichment of incompatible elements. Trace elements were normalized to average compositions of different magmatic arcs and mid-ocean ridge basalts for comparison, following the method of Philbrick (2016). Rare earth element (REE) diagrams, illustrating the normalized data, are presented in Figures 17-18, with compatibility of elements increasing to the right. Figure 17 represents the mean values of the lower Boone, upper Boone, and Arkansas Novaculite REE concentration normalized to average continental arc composition (Keleman et al., 2004). Figure 18 represents the mean of each interval REE concentration normalized to average mid-ocean ridge basalts (Kelemen et al., 2004). Trace element data were also normalized to Post-Archean Australian Shales (PAAS) and plotted on diagrams of rare earth elements plus yttrium (Figure 19).

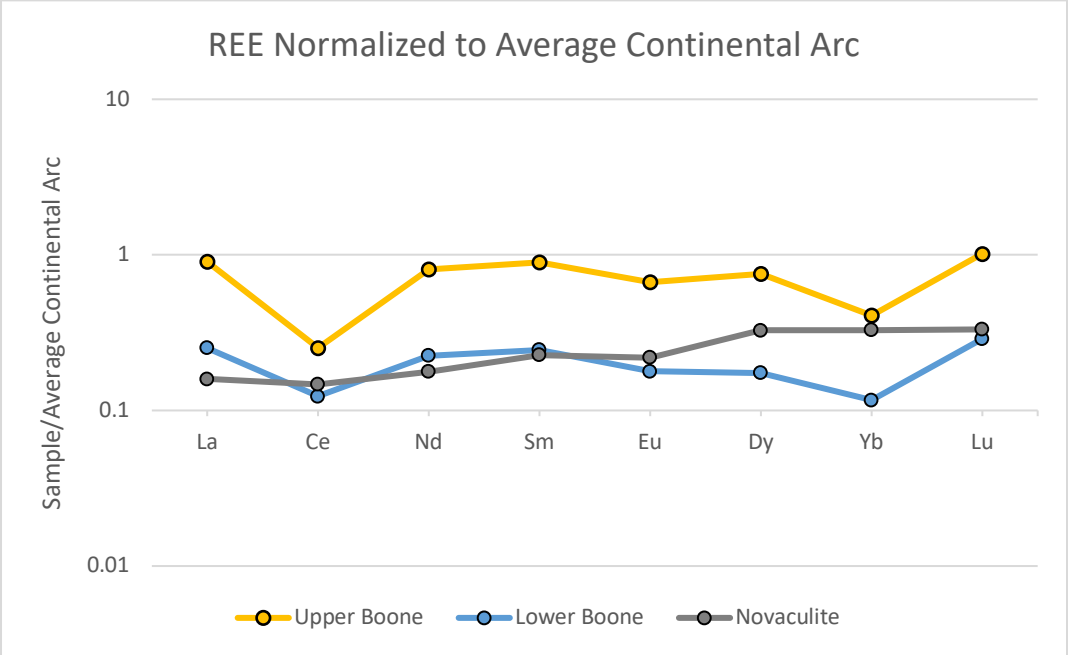

Figure 17. REE diagrams depicting averaged sample concentrations for the lower Boone, upper Boone, and Arkansas Novaculite relative to average continental arc (continental arc data from Keleman et al., 2004).

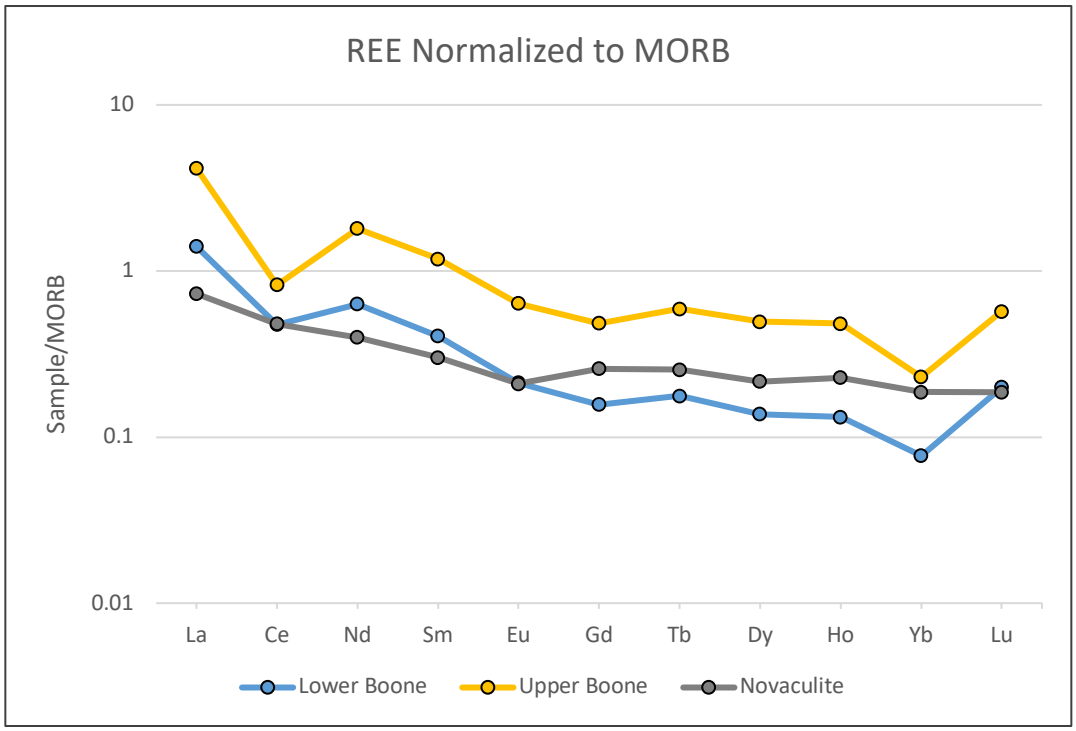

Figure 18. REE diagrams depicting averaged sample concentrations for the lower Boone, upper Boone, and Arkansas Novaculite relative to MORB (MORB data from Kelemen et al., 2004).

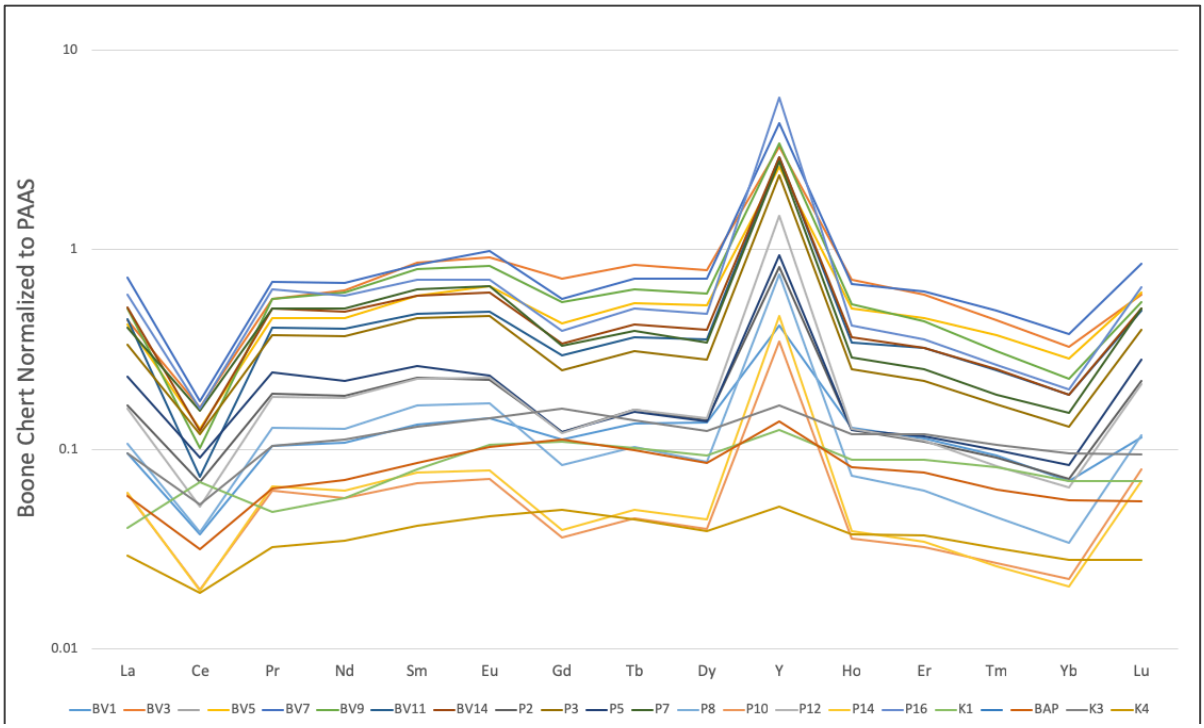

Figure 19. REY diagram of Boone chert samples normalized to PAAS (Pourmand et al., 2012). Note negative cerium anomaly and positive Y anomaly.

8.2 X-ray Diffraction

X-ray diffraction (XRD) data are presented in Figures 20-24. Mineral percentages for chert and novaculite samples are represented in pie charts. The XRD pattern for sample P2, a penecontemporaneous Boone chert from Pineville, Arkansas, is shown in Figure 20. The XRD reveals it is comprised of 97% silica, 2% calcite, and 1% dolomite. The Arkansas Novaculite samples consist of varying amounts of silica, calcite, and dolomite (Figures 21-22). The Hatton Tuff samples are composed of quartz and feldspar (Figures 23-24).

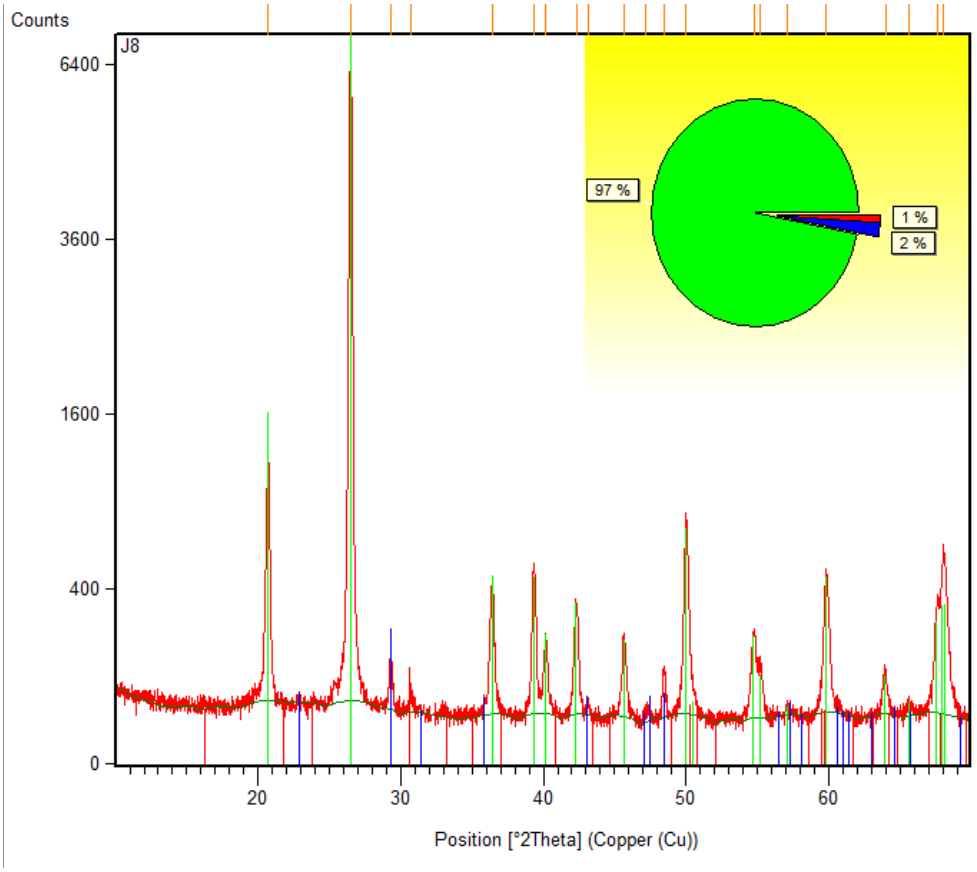

Figure 20. XRD analysis for sample P2 (lower Boone, penecontemporaneous chert, from Pineville, Arkansas) showing 97% silica, 2% calcite, and 1% dolomite.

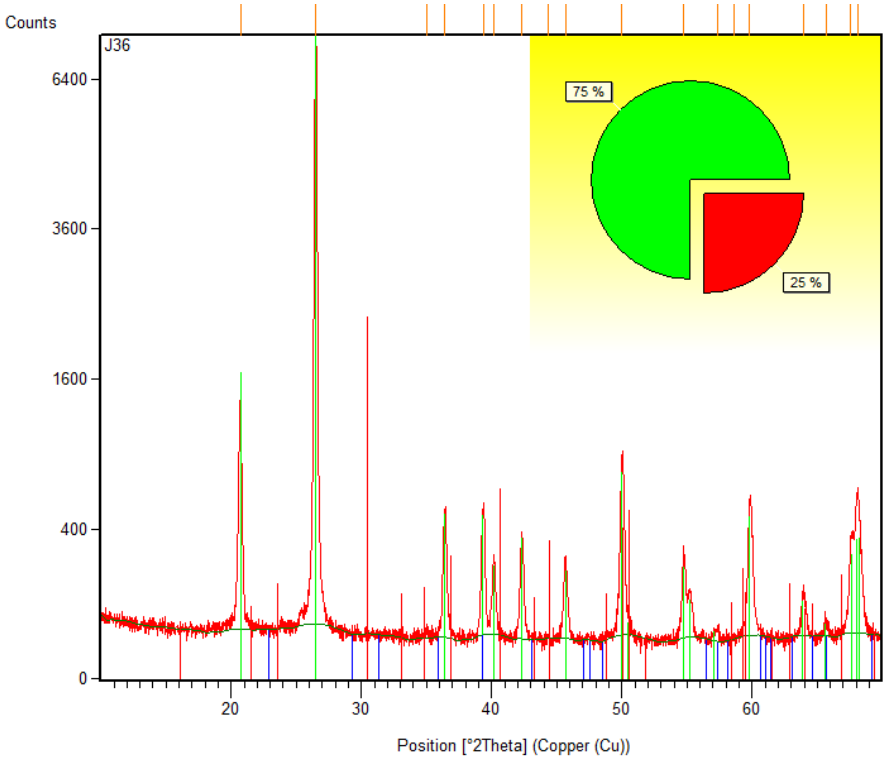

Figure 21. Sample CG71 (upper Arkansas Novaculite; Caddo Gap roadcut) XRD data. Green indicates that sample is 75% silica and red indicates 25% dolomite.

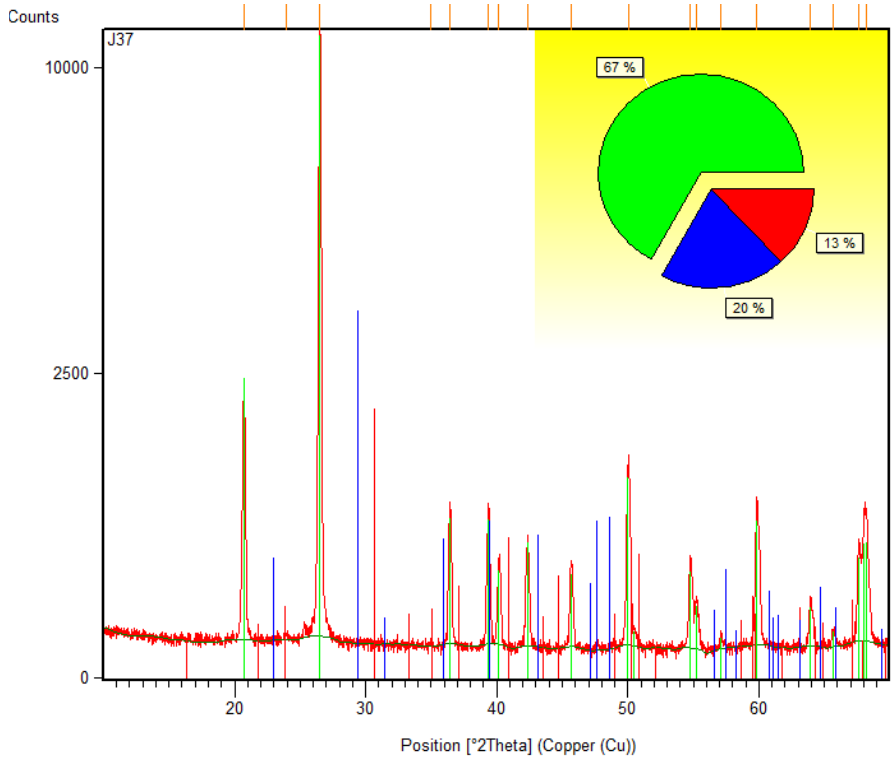

Figure 22. Sample CG77 (upper Arkansas Novaculite; Caddo Gap roadcut) XRD data. Green indicates that sample is 67% silica, blue indicates 20% calcite, and red indicates 13% dolomite.

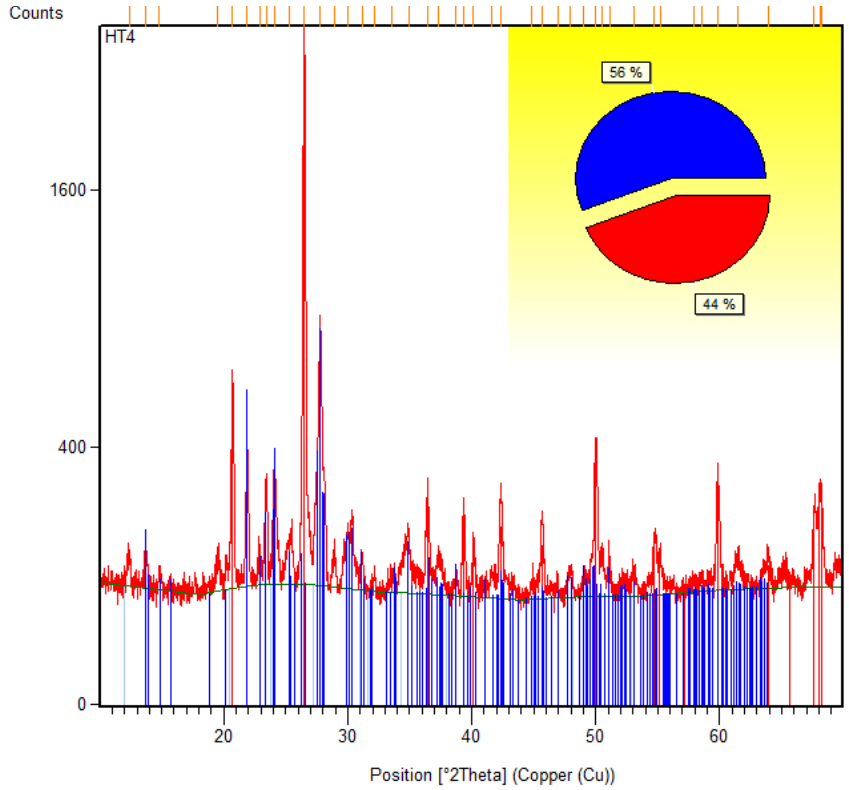

Figure 23. Sample HT4 (Hatton Tuff; Hatton, AR) XRD data. Blue indicates 56% quartz content and red indicates 44% feldspar content.

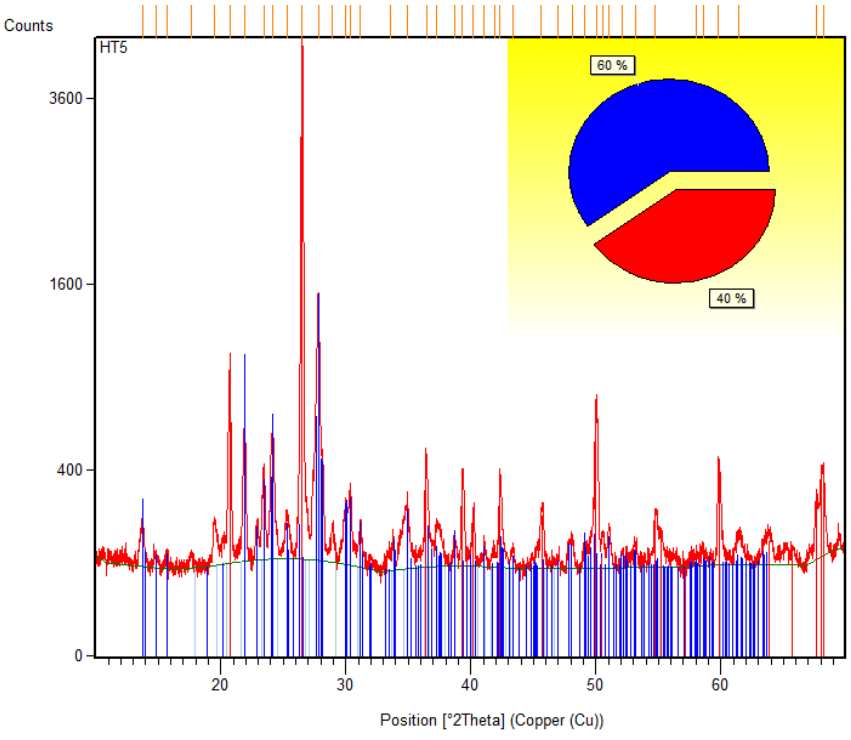

Figure 24. Sample HT5 (Hatton Tuff; Hatton, AR) XRD data. Blue indicates 60% quartz content and red indicates 40% feldspar content.

8.3 Lead Isotopes

Lead isotope ratios of the 33 rock samples analyzed in this study are reported in Tables 2 and 3. Table 2 represents the present day Pb isotope ratios for all of the samples. The lower Boone cherts have a measured present day Pb isotope range of 18.8345 to 21.3028 for $^{206}Pb/^{204}Pb$, a range of 15.6599 to 15.8429 for $^{207}Pb/^{204}Pb$, and a range of 38.6232 to 40.1589 for $^{208}Pb/^{204}Pb$ (Table 2). The upper Boone cherts present day Pb isotope ratios have a range of 21.0044 to 22.9937 for $^{206}Pb/^{204}Pb$, 15.7962 to 15.9390 for $^{207}Pb/^{204}Pb$, and 39.4391 to 40.4346 for $^{208}Pb/^{204}Pb$. The Arkansas Novaculite samples display wide ranges of Pb isotope ratios. The lower Arkansas Novaculite interval displays an isotopic range of 18.7759 to 29.5943 for $^{206}Pb/^{204}Pb$, 15.6607 to 15.2598 for $^{207}Pb/^{204}Pb$, and 28.6416 to 39.3755 for $^{208}Pb/^{204}Pb$. The upper Arkansas Novaculite interval ranges 18.9189 to 25.5943 for $^{206}Pb/^{204}Pb$, 15.6671 to 16.2598 for $^{207}Pb/^{204}Pb$, and 38.6353 to 39.3755 for $^{208}Pb/^{204}Pb$. The two Hatton Tuff samples measured 19.0531 and 19.5468 for $^{206}Pb/^{204}Pb$, 15.6687 and 15.6904 for $^{207}Pb/^{204}Pb$, and 39.1791 and 40.0042 for $^{208}Pb/^{204}Pb$. The St. Joe chert sample measured 19.2449 for $^{206}Pb/^{204}Pb$, 15.6871 for $^{207}Pb/^{204}Pb$, and 38.7455 for $^{208}Pb/^{204}Pb$. The Pitkin chert sample measured 21.6314 for $^{206}Pb/^{204}Pb$, 15.8259 for $^{207}Pb/^{204}Pb$, and 39.2772 for $^{208}Pb/^{204}Pb$. All of the Pb isotope ratios were age corrected to 250 million years (Table 3; Pb, Th, and U concentrations used for age corrections are found in Appendix 2.1), corresponding to the precipitation of the ores, allowing comparison with the ore deposits and evaluation of the potential genetic relationship between the siliceous deposits and the ores. Figures 25 and 26 are covariate diagrams displaying the Pb isotope ratios of the samples analyzed in this study, in conjunction with the Pb isotope ratios of ores from the Northern Arkansas and the Tri-State MVT mining districts. Also plotted is Zartman and Doe's (1981) model for the upper crust and the orogenic growth curves.

Table 2. Present day Pb isotope ratios.

Outcrop Label	Formation/Member	208/204 Pb	207/204 Pb	206/204 Pb
BAP	St Joe: Pierson	38.7455	15.6871	19.2449
P2	Lower Boone	39.7230	15.7851	20.4621
P3	Lower Boone	39.6222	15.7905	20.4977
P4	Lower Boone	39.6771	15.7838	20.4691
P5	Lower Boone	39.7233	15.7809	20.4137
P7	Lower Boone	40.1589	15.8384	21.0689
P7	Lower Boone	40.1493	15.8350	21.0714
P8	Lower Boone	40.1464	15.8372	21.2575
P10	Lower Boone	40.1156	15.8429	21.3028
P12	Lower Boone	40.0721	15.8428	21.2658
K1	Lower Boone	38.6232	15.6599	18.8345
K3	Lower Boone	38.8602	15.7071	19.5607
K4	Lower Boone	39.1076	15.7538	20.3320
BV1	Upper Boone	40.1788	15.8970	22.2969
BV3	Upper Boone	40.4346	15.8959	21.9110
BV5	Upper Boone	40.3212	15.9390	22.9937
BV7	Upper Boone	40.0450	15.8994	22.6978
BV11	Upper Boone	39.4391	15.7962	21.0044
BV14	Upper Boone	39.6893	15.8271	21.6243
P14	Elsey	40.0391	15.8379	21.3534
P16	Elsey	40.2242	15.8643	21.7211
Pit1	Pitkin	39.2772	15.8259	21.6314
HT4	Hatton Tuff	39.1791	15.6687	19.0531
HT5	Hatton Tuff	40.0042	15.6904	19.5468
CG6	Lower Novaculite	38.9604	15.6607	18.7759
CG8	Lower Novaculite	38.9528	15.6768	19.0813
CG18	Lower Novaculite	39.6727	15.7861	20.8876
CG39	Lower Novaculite	42.4587	15.9955	25.1670
CG52	Lower Novaculite	38.6416	15.8793	22.6982
CG71	Upper Novaculite	38.7656	16.2598	29.5943
CG82	Upper Novaculite	38.6353	15.7689	20.7863
CG85	Upper Novaculite	39.2452	15.7989	21.5355
CG86	Upper Novaculite	38.8443	15.6671	18.9189

Table 3. Pb isotope ratios, age corrected to 250 million years.

Outcrop Label	Formation/Member	$^{206}Pb/^{204}$ Pb	$^{207}Pb/^{204}Pb$	$^{208}Pb/^{204}Pb$
		Age Corrected 250 million years		
BAP	St Joe: Pierson	18.892898	15.669069	38.695059
P2	Lower Boone	20.155393	15.769355	39.609766
P3	Lower Boone	20.002065	15.765109	39.485923
P4	Lower Boone	20.147826	15.767313	39.570401
P5	Lower Boone	20.786602	15.823900	40.066574
P7	Lower Boone	20.935281	15.820739	40.038734
P8	Lower Boone	20.832318	15.818791	40.012269
P12	Lower Boone	20.612029	15.809312	39.859343
K1	Lower Boone	18.555123	15.645642	38.438523
K3	Lower Boone	19.147965	15.685976	38.731585
K4	Lower Boone	20.048180	15.739303	39.028349
BV1	Upper Boone	21.403473	15.851287	39.985457
BV3	Upper Boone	21.514446	15.875628	40.344595
BV5	Upper Boone	21.854010	15.880650	39.966447
BV7	Upper Boone	20.266672	15.774925	39.506423
BV11	Upper Boone	19.784524	15.733692	39.181154
BV14	Upper Boone	19.917084	15.739643	39.226603
P14	Upper Boone/Elsey	20.885676	15.813984	39.903626
P16	Upper Boone/Elsey	20.624108	15.808156	39.940828
Pit1	Pitkin	19.536266	15.718593	38.611652
CG6	Lower Novaculite	18.494020	15.646235	38.600460
CG8	Lower Novaculite	18.593753	15.651806	38.585075
CG18	Lower Novaculite	19.882847	15.734679	38.918423
CG39	Lower Novaculite	19.846389	15.723039	39.303454
CG52	Lower Novaculite	20.250793	15.754024	38.437124
CG71	Upper Novaculite	21.666286	15.853874	38.500240
CG82	Upper Novaculite	19.955616	15.726368	38.544676
CG85	Upper Novaculite	20.072312	15.724015	38.460074
CG86	Upper Novaculite	18.611024	15.651358	38.493101

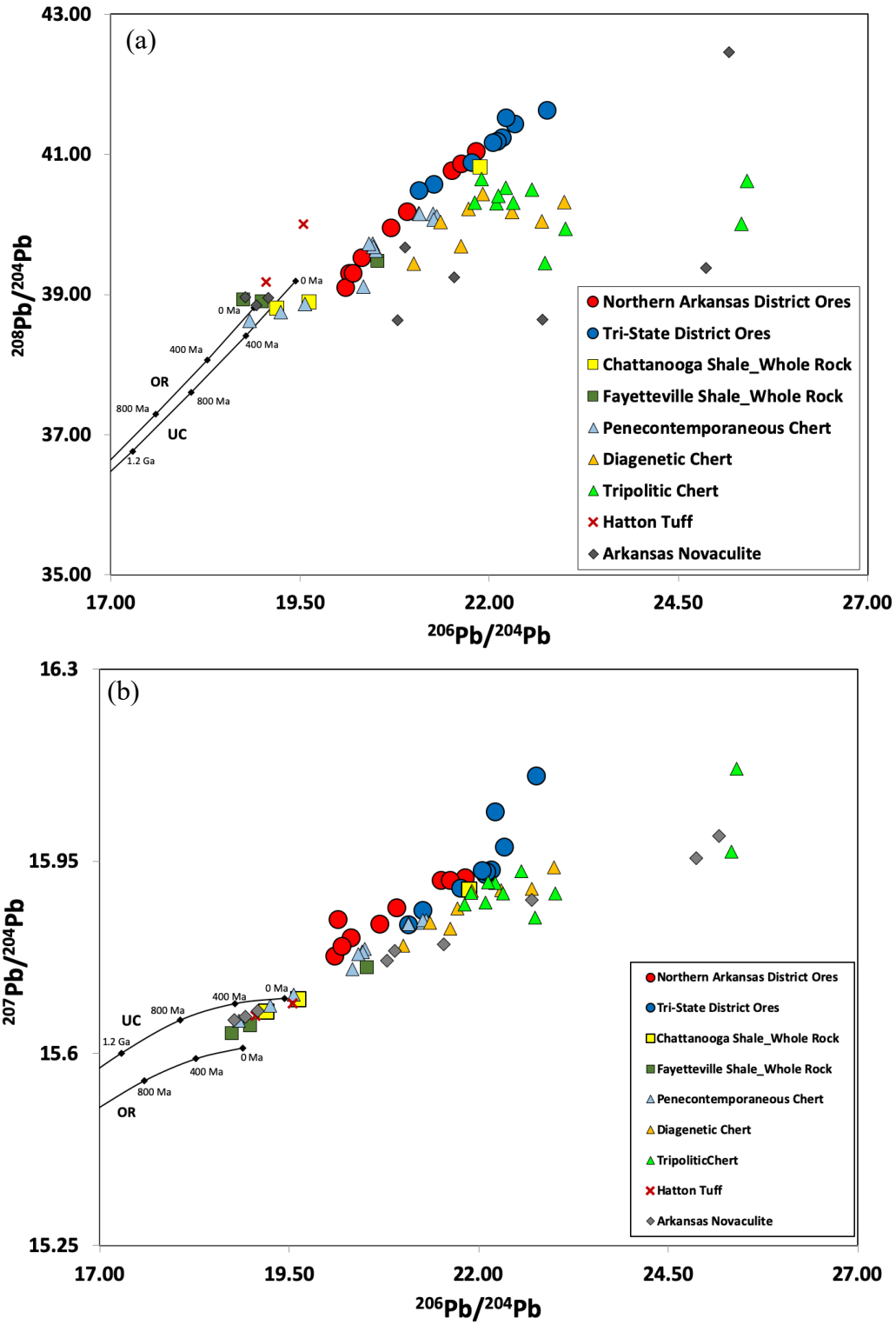

Figure 25. Covariate diagrams (a-thorogenic; b-uranogenic) displaying the present day Pb isotope ratios for samples analyzed in this study, in conjunction with the Northern Arkansas District and Tri-state District ore values (Potra et al., 2018; Bottoms et al., 2019), tripolitic chert samples (McKim, 2018), shale samples (Bottoms et al., 2019), and Zartman and Doe's (1981) model for upper crust (UC) and the orogenic growth curve (OR).

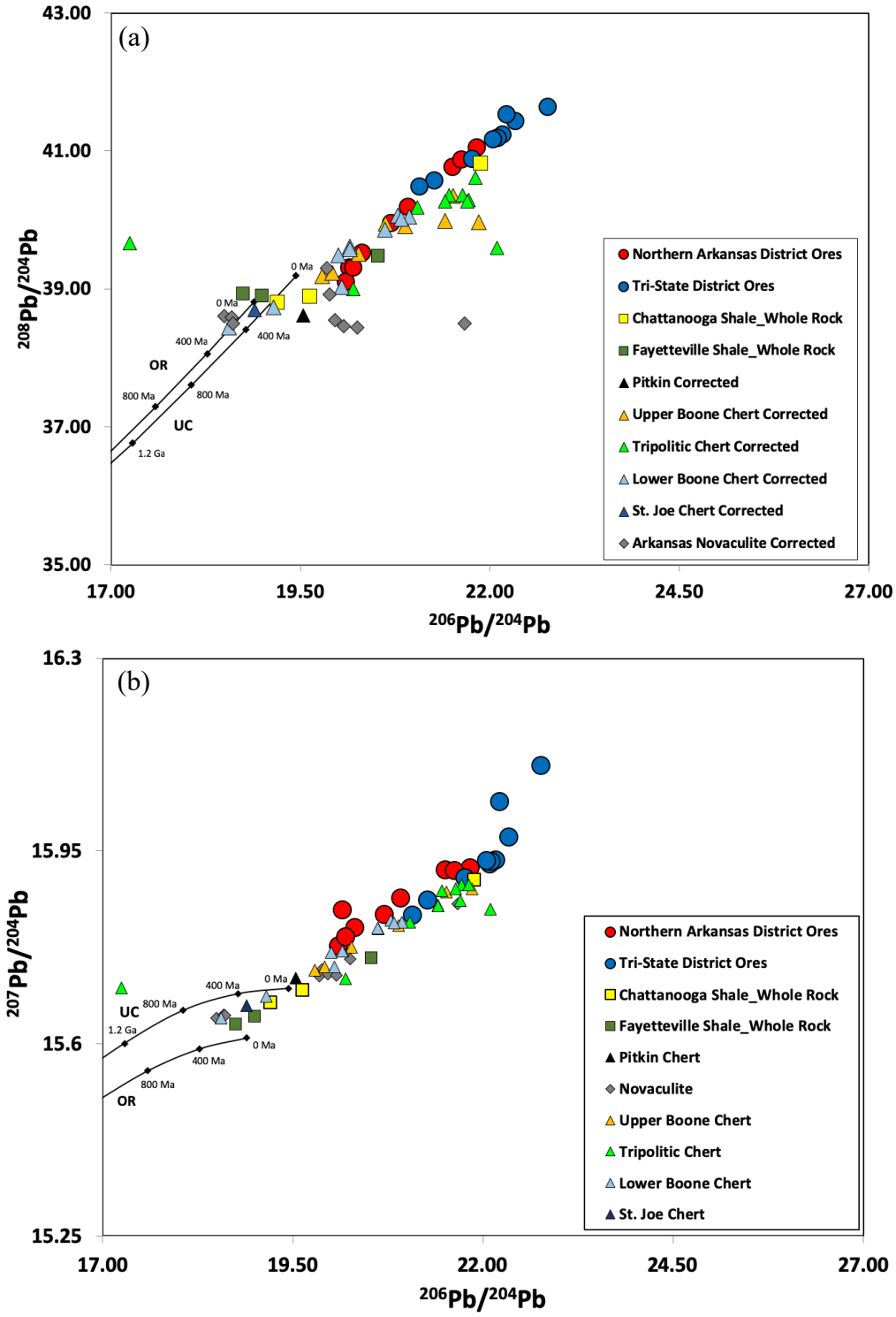

Figure 26. Age corrected Pb isotope data, corrected to 250 million years. Data plotted in conjunction with the Northern Arkansas District and Tri-state District ore values (Potra et al., 2018; Bottoms et al., 2019), tripolitic chert samples (McKim, 2018), shale samples (Bottoms et al., 2019), as well as Zartman and Doe's (1981) model for upper crust (UC) and the orogenic growth curve (OR).

8.4 Strontium and Neodymium Isotopes

Table 4 compiles the measured Sr and Nd isotope ratios for samples analyzed in this study. The lower Boone cherts have a measured range of 0.708212 to 0.714981 for ^{87}Sr / ^{86}Sr and 0.512105 to 0.512202 for ^{143}Nd / ^{144}Nd. The upper Boone cherts have a range of 0.708727 to 0.709322 for ^{87}Sr / ^{86}Sr and 0.509752 to 0.512271 for ^{143}Nd / ^{144}Nd. The lower Novaculite interval displays a range of 0.714738 to 0.724588 for ^{87}Sr / ^{86}Sr and 0.512001 to 0.512180 for ^{143}Nd / ^{144}Nd. The upper Novaculite interval displays a range of 0.712124 to 0.717451 for ^{87}Sr / ^{86}Sr and 0.512090 to 0.512230 for ^{143}Nd / ^{144}Nd. The two Hatton Tuff samples measured 0.737447 and 0.736163 for ^{87}Sr / ^{86}Sr and 0.512264 and 0.512238 for ^{143}Nd / ^{144}Nd. The St. Joe chert sample measured 0.710304 for ^{87}Sr / ^{86}Sr and 0.512197 for ^{143}Nd / ^{144}Nd. The Pitkin chert sample measured 0.708739 for ^{87}Sr / ^{86}Sr and 0.512098 for ^{143}Nd / ^{144}Nd.

The Sr and Nd isotope data were age corrected for 350 million years, corresponding to the approximate time of deposition. These data are compiled in Table 5. Detailed Sr and Nd isotope ratios and the associated errors can be found in the Appendix. The epsilon value for Nd was calculated using age corrected data, which expresses the deviation of the Nd isotope ratios from the chondritic uniform reservoir (CHUR) evolution line using the following formula (Dickin, 2005):

$$\varepsilon\, Nd\ (t) = \left(\frac{(^{143}Nd/^{144}Nd)_{sample}(t)}{^{143}Nd/^{144}Nd)_{CHUR}(t)} - 1 \right) x\ 10^4$$

where *t* indicates the time for which $\varepsilon\, Nd$ is calculated. These values are plotted in Figure 28, in conjunction with Ordovician (Mazarn, Womble, and Polk Creek) shales (Simbo, 2019), the Pennsylvanian Jackfork Sandstone (Simbo, 2019), the Devonian/Mississippian Chattanooga Shale (Bottoms, 2017), the Mississippian Fayetteville Shale (Bottoms, 2017), and Cretaceous alkaline igneous rocks from Magnet Cove (carbonatite) and Granite Mountain (syenite) in

Arkansas (Groh et al., 2017; Potra et al., 2017). A table of epsilon values and the ages used for correction can be found in Appendix 3.4.

Table 4. Present day Sr and Nd isotopic ratios.

Outcrop Label	Formation/Member	87/86 Sr	143/144 Nd
BAP	St Joe: Pierson	0.710304	0.512197
P2	Lower Boone	0.711023	0.512152
P3	Lower Boone	0.708212	0.512185
P4	Lower Boone	0.711020	0.512135
P5	Lower Boone	0.714478	0.512105
P7	Lower Boone	0.710492	0.512146
P7	Lower Boone	0.710519	0.512152
P8	Lower Boone	0.710546	0.512161
P10	Lower Boone	0.709748	0.512177
P12	Lower Boone	0.708290	0.512187
K1	Lower Boone	0.710988	0.512202
K3	Lower Boone	0.712938	0.512158
K4	Lower Boone	0.714981	0.512156
BV1	Upper Boone	0.709098	0.512191
BV3	Upper Boone	0.708867	0.509752
BV5	Upper Boone	0.708916	0.512257
BV7	Upper Boone		0.512225
BV11	Upper Boone	0.708727	0.510181
BV14	Upper Boone	0.709322	0.512271
P14	Upper Boone/Elsey	0.708822	0.512179
P16	Upper Boone/Elsey	0.709014	0.512223
Pit1	Pitkin	0.708739	0.512098
HT4	Hatton Tuff	0.737447	0.512264
HT5	Hatton Tuff	0.736163	0.512238
CG6	Lower Novaculite	0.724588	0.512022
CG8	Lower Novaculite	0.719874	0.512001
CG18	Lower Novaculite	0.714738	0.512035
CG39	Lower Novaculite	0.717184	0.512041
CG52	Lower Novaculite	0.716938	0.512180
CG71	Upper Novaculite	0.714945	0.512090
CG82	Upper Novaculite	0.715391	0.512221
CG85	Upper Novaculite	0.713192	0.512198
CG86	Upper Novaculite	0.717451	0.512230

Table 5. Age corrected Sr and Nd isotope ratios.

Outcrop Label	Formation/Member	87/86 Sr	143/144 Nd
		Age Corrected 350 million years	
BAP	St Joe: Pierson	0.709000386	0.511922572
P2	Lower Boone	0.709401	0.511872
P3	Lower Boone	0.707945	0.511907
P4	Lower Boone	0.709743	0.511837
P5	Lower Boone	0.708971	0.511862
P7	Lower Boone	0.708974	0.511867
P8	Lower Boone	0.708724	0.511908
P12	Lower Boone	0.707979651	0.511903471
K1	Lower Boone	0.709659361	0.511887086
K3	Lower Boone	0.709229485	0.511894315
K4	Lower Boone	0.709300589	0.511887825
BV1	Upper Boone	0.708937	0.511916
BV3	Upper Boone	0.708666	0.509441
BV5	Upper Boone	0.708779	0.511967
BV7	Upper Boone		0.511948
BV11	Upper Boone	0.708616	0.509914
BV14	Upper Boone	0.709070	0.512002
P14	Upper Boone/Elsey	0.708142414	0.511901228
P16	Upper Boone/Elsey	0.708887829	0.511953052
CG6	Lower Novaculite	0.715696685	0.51169586
CG8	Lower Novaculite	0.714716729	0.511700699
CG18	Lower Novaculite	0.712710362	0.511774866
CG39	Lower Novaculite	0.713538438	0.511742986
CG52	Lower Novaculite	0.712149026	0.511849054
CG71	Upper Novaculite	0.711587831	0.511773498
CG82	Upper Novaculite	0.71155366	0.511914033
CG85	Upper Novaculite	0.711064457	0.511882562
CG86	Upper Novaculite	0.712136047	0.511905056
		Age corrected 325 million years	
Pit1	Pitkin	0.708213632	0.511846823

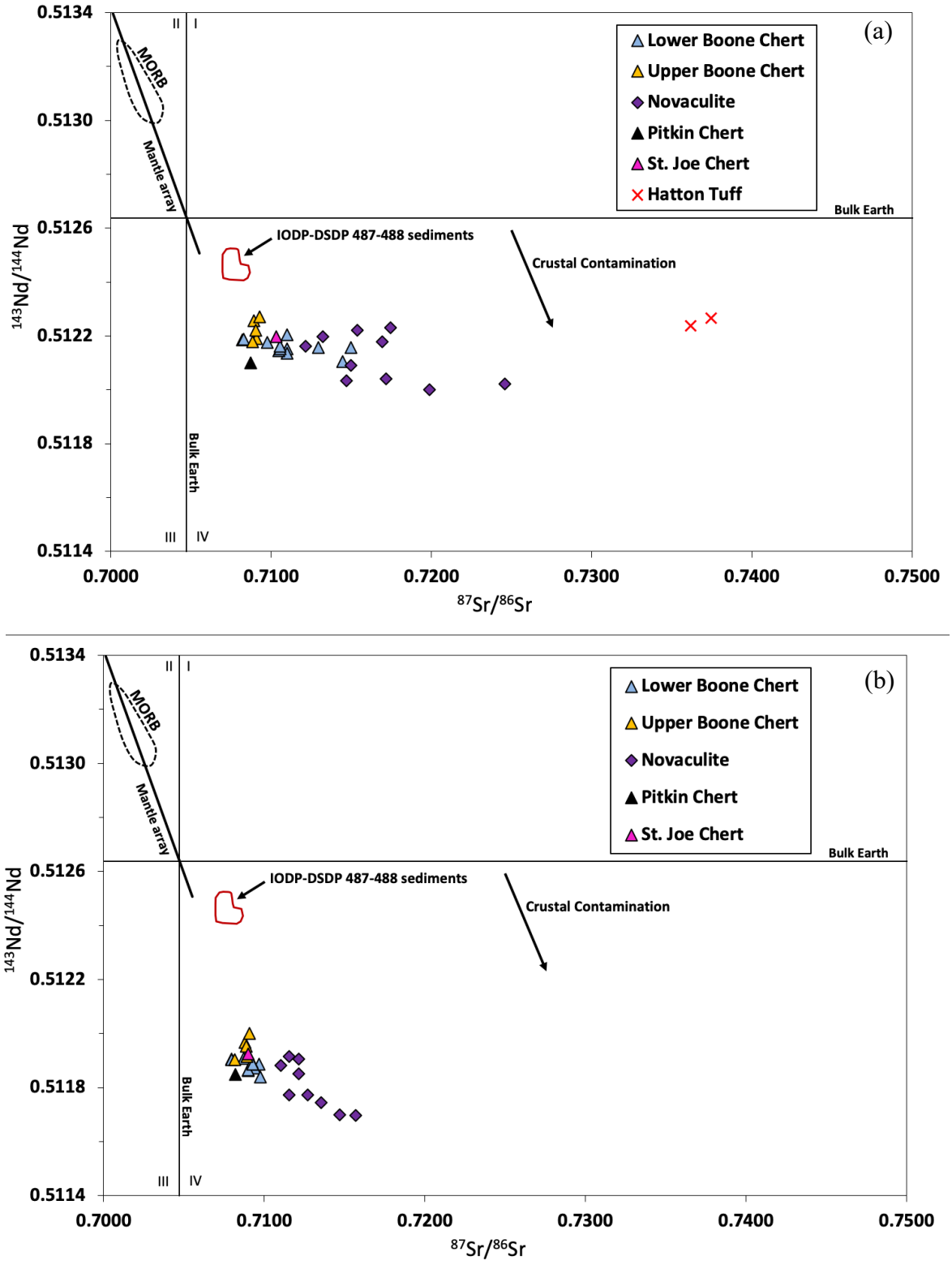

Figure 27. Present day (a) and initial (b) Nd versus Sr isotope ratios, plotted in conjunction with the mantle array and isotope fields for MORBs and IODP-DSDP 487-488 sediments (Verma, 2000).

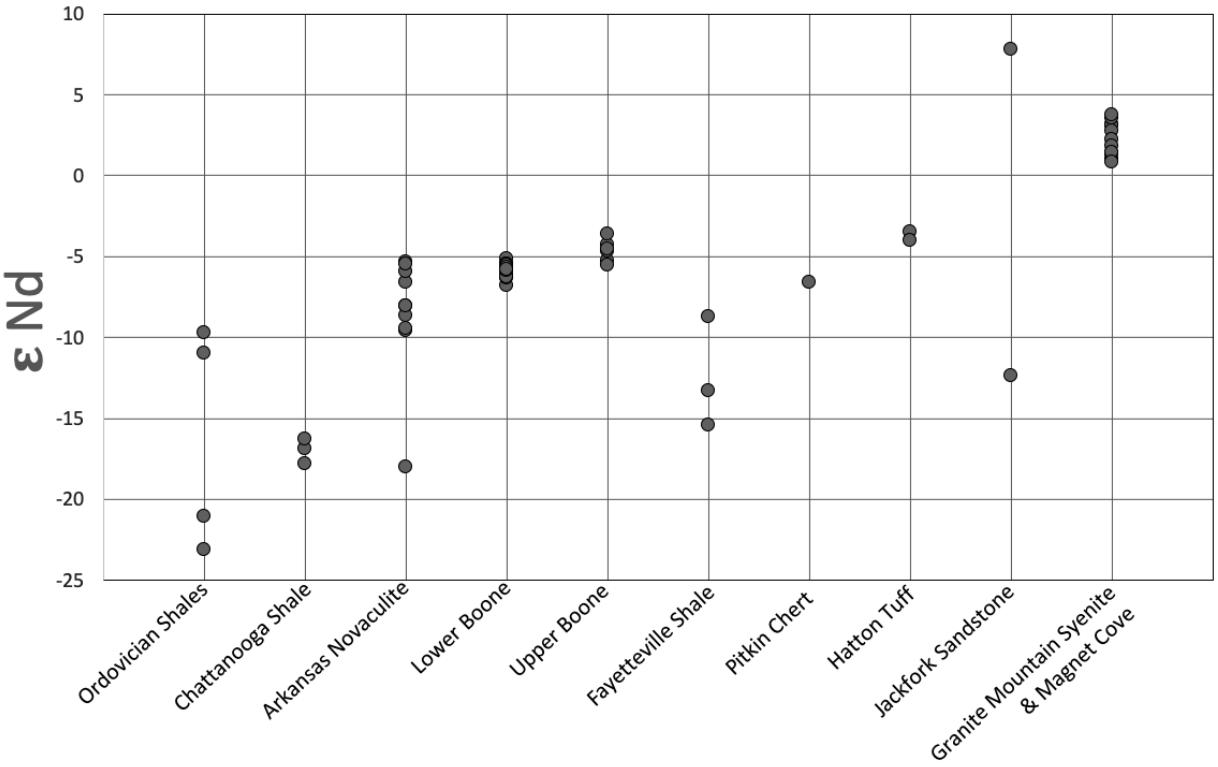

Figure 28. Epsilon values calculated using Nd isotope ratios age corrected to approximate time of deposition for Ordovician (Mazarn, Womble, and Polk Creek) shales (Simbo, 2019), the Pennsylvanian Jackfork Sandstone (Simbo, 2019), the Devonian/Mississippian Chattanooga Shale (Bottoms, 2017), the Mississippian Fayetteville Shale (Bottoms, 2017), and Cretaceous alkaline igneous rocks from Magnet Cove (carbonatite) and Granite Mountain (syenite) in Arkansas (Groh et al., 2017; Potra et al., 2017).

9. DISCUSSION

9.1 Trace Elements

The REE are among the least soluble of the trace elements and have been shown to be relatively immobile during low-grade metamorphism, weathering, and hydrothermal alteration (Michard, 1989). However, the variable oxidation states of Ce and Eu make them more mobile than the other REE under certain conditions (Hollings and Wyman, 2004). Cerium, for instance, shows both depletions and enrichments during oxidative weathering, while Eu may be depleted in oxidizing environments and enriched under reducing conditions (Hollings and Wyman, 2004). Carbonate alteration seems to result in greater mobility of all REE (Hynes, 1980). These are just some cautionary words to consider when interpreting trace element patterns in sedimentary systems.

Trace element data normalized to average continental arc (Figure 17), MORB (Figure 18), and PAAS (Figure 19) concentrations and plotted on spider diagrams reveal relative enrichment or depletion of incompatible elements (incompatibility increases from the right side to the left side of the diagrams) and provide source implications. A negative trend observed in the REE values normalized to MORB (Figure 18) indicates that the siliceous rocks analyzed in this study are enriched in more incompatible elements rather than less incompatible elements relative to MORB. In the case of the Boone chert samples, the normalized values of the most incompatible element (La) is higher than 1. A slightly different pattern is recorded for the Arkansas Novaculite, with all of the normalized values lower than 1, suggesting that the Boone chert samples originate from more evolved sources compared to the Arkansas Novaculite samples. Also, this points to an enriched source of the Boone chert relative to MORB, which originates from a depleted mantle source.

When normalized to continental arc concentrations (Figure 17), the samples analyzed in this study have a relatively flat signature, with all of the normalized values lower than 1. However, the upper Boone samples normalized to continental arc concentrations plot very near a value of 1, indicating similar compositions. The lower Boone and the Arkansas Novaculite samples have lower normalized values. This may be a function of lithology and the ability of silica versus calcite to incorporate trace elements. The upper Boone chert is a replacement of limestone, so the trace element concentrations may reflect the original limestone depositional characteristics. The overall trend suggests a less evolved source compared to continental arc rocks. However, the Arkansas Novaculite samples show a slight positive trend, with enrichment of less incompatible elements. Similar to the MORB normalized REE values, the continental arc normalized REE values of the Arkansas Novaculites point to a less evolved source compared to the Boone chert samples.

The majority of the Boone chert samples display a negative Ce anomaly when normalized to the Post-Archean Australian Shale (PAAS) data (Figure 19). Cerium (Ce) in the oceans is scavenged by Fe-Mn nodules and oxide/hydroxide crusts, which causes a depletion of Ce in minerals that are directly precipitated from seawater (Faure, 1977). The Boone chert samples also have a positive Y anomaly, which is a signature of modern seawater (Tostevin et al., 2016). The Ce and Y anomalies indicate that the Boone Formation cherts may retain the seawater trace element concentrations from the time of their deposition.

9.2 Lead Isotopes

Lead (Pb) has four stable isotopes, only one of (^{204}Pb) which is nonradiogenic (Dickin, 2005). The other three stable Pb isotopes result from the decay of uranium and thorium. ^{238}U ultimately decays to ^{206}Pb, ^{235}U decays to ^{207}Pb, and ^{232}Th decays to ^{208}Pb (Dickin, 2005). Figures 25a and 26a are called thorogenic diagrams, because they show ^{208}Pb/^{204}Pb ratios versus

$^{206}Pb/^{204}Pb$, and Figures 25b and 26b are uranogenic diagrams because they compare $^{207}Pb/^{204}Pb$ versus $^{206}Pb/^{204}Pb$. Plotted in conjunction with the data on Figures 25 and 26 are Zartman and Doe's (1981) orogenic growth curve and upper crust growth curve, which represent the Pb isotope composition of orogenic regions and the upper crust through time as radioactive U and Th decay into their radiogenic daughters. By plotting the Pb isotope ratios, a comparison between the relative enrichment of radiogenic Pb of the analyzed samples and the isotope composition of these two reservoirs can be determined.

On Figures 25 and 26, it is clear that the ore deposits in both the Northern Arkansas and Tri-State districts are enriched in radiogenic Pb. The ores contain a range of Pb isotope ratios, which form linear trends. The linear trends are usually interpreted as the mixing of two end member components, or from a single source of Pb that contains variable Pb isotope compositions. The Pb in a particular interval would need to fall along the same trend as the ore deposits in order to be considered a viable source for the metals.

The majority of the Boone chert samples analyzed in this study contain highly radiogenic Pb with isotopic ratios comparable to the MVT ore deposits in the Northern Arkansas and Tri-State districts. This strongly suggests a genetic relationship between some of the Boone chert and the ore deposits, which can be interpreted in two ways: either the Boone Formation acted as a Pb source for the ore deposits, or the hydrothermal fluids contaminated the Boone Formation with radiogenic Pb. If the Boone Formation was the source of the radiogenic Pb in the ores, then the Pb in the Boone may reflect seawater Pb during the time of deposition. Since Pb has a very short residence time in the oceans (~50 years, Craig et al. 1973), it may be expected that the record of Pb isotope composition of the oceans would show rapid changes (Dickin, 2005). Basement rocks or sedimentary rocks derived from the basement are indicated as a source for metals in many MVT ore deposits (Leach, 2010). It seems probable that siliciclastic rocks comprising weathered

continental rock would contain radiogenic Pb. It seems less likely that radiogenic Pb would have been incorporated into carbonates and penecontemporaneous chert, unless the Pb isotope composition of seawater at the time of deposition reflected radiogenic Pb input. Another issue with proposing the Boone Formation as a Pb source for the ores is the low concentration of Pb in the Boone cherts (average 2ppm Pb). It is recommended that the limestone in the Boone Formation should be analyzed for Pb concentration and Pb isotope ratios for comparison to the chert and to determine whether the radiogenic Pb is exclusive to the silicified intervals.

Part of the objective of this thesis is to evaluate the potential of silica contribution in the form of volcanic ash, leading to the formation of the penecontemporaneous and later diagenetic chert in the Boone Formation. These two chert types formed very differently from the tripolitic chert in the Boone Formation, and two points must be made to clarify the relationship between the cherts and timing of formation. First, MVT ore deposits are unrelated to igneous activity, so the emplacement of the ores and the tripolitic chert should not necessarily reflect volcanic ash contribution (unless there was chert present prior to hydrothermal fluid contact). The ore deposits are dated as Permian, which is significantly younger than the deposition of the Boone Formation. Therefore, the lower Boone penecontemporaneous chert and later diagenetic chert would likely have different Pb sources and Pb isotope signatures than the ores and tripolitic chert. Second, Pb isotope signatures that are more radiogenic are typically indicative of input from old continental sources, whereas Pb sourced from volcanic activity is less radiogenic. The Hatton Tuff samples analyzed in this study support this contention. The tuff sample HT4 plots with the less radiogenic samples, and HT5 is slightly more radiogenic, still significantly less radiogenic than the tripolitic chert. It must be noted that the Hatton Tuff samples are only plotted with present day values due to a lack of concentration data that are used for age correction. It appears that the highly radiogenic Pb emplaced by hydrothermal fluids was likely scavenged from sedimentary rocks

through which the fluids traveled cratonwards, away from the orogenic belt. Bottoms et al. (2019) evaluated the Chattanooga Shale and Fayetteville Shale as potential sources for the metals in the ore deposits. The authors found that the Pb in those intervals was not radiogenic enough to be the more radiogenic component of the ore Pb. They concluded that the shales, in particular the Chattanooga Shale, may represent the non-radiogenic end member that contributed Pb to the ores.

The most pure, unaltered, penecontemporaneous chert samples (K1, K3, BAP, Pit1) from Kansas (Oklahoma), Branson Airport, and Deer contain the least radiogenic Pb of all chert samples. The lower Boone cherts from the Pineville roadcut that are also relatively pure and unaltered (P2, P3, P4) are slightly more radiogenic, but still significantly less radiogenic than the tripolitic cherts. The lower Boone chert samples from Pineville that contain a mixture of dark and white chert are very radiogenic and display Pb isotope signatures comparable to the ores. These samples are higher in the stratigraphic section, closer to the tripolitized interval, and could have been influenced by the hydrothermal fluids passing through, the same hydrothermal fluids that generated the ores.

Although the Pb isotope ratios in the diagenetic chert of the upper Boone vary greatly, a pattern is present. The diagenetic chert that was sampled near the boundary of the tripolitic chert interval (P14, P16, BV1, BV3, BV5) contains radiogenic lead comparable to that of the tripolitic chert. In contrast, the diagenetic chert well above the tripolitic interval (samples BV7, BV11, and BV14, which are 9ft, 30ft, and 47ft above the tripolitic chert, respectively) is much less radiogenic. This indicates that the hydrothermal fluids that replaced the limestone in the Boone Formation and emplaced the tripolitic chert interval likely altered the surrounding rock and also contaminated the upper and lower Boone with radiogenic Pb outside the main zone of alteration. It also indicates that the hydrothermal fluids that emplaced the tripolitic chert contained more

radiogenic Pb than the fluids that emplaced the later diagenetic chert. The later diagenetic chert only occurs along bedding planes, and is interpreted as groundwater replacement of limestone.

The present day Pb isotope ratios of the Arkansas Novaculite are highly variable and show a mixture of very radiogenic and much less radiogenic Pb (Figure 25). Upon age correction, the data display a much less radiogenic signature and plot near the upper crust and orogenic growth curves (Figure 26). The age corrected novaculite samples contain Pb that is significantly less radiogenic than the tripolitic chert, plotting very close to the pure penecontemporaneous cherts and the present-day Hatton Tuff samples. This indicates that the novaculite did not act as a source for radiogenic Pb in the ores and does not contain hydrothermally emplaced radiogenic Pb.

The Pb isotope data neither preclude nor confirm the input of volcanic ash as a silica source. Using silicon isotope analysis, future studies should evaluate the potential of igneous activity to have contributed silica to the Boone chert and Arkansas Novaculite. Therefore, volcanic ash remains as a potential contributor to the silica comprising the pure cherts and the less radiogenic diagenetic cherts. The fact that these cherts have less radiogenic Pb, however, does not confirm that volcanic ash was the silica source. The Chattanooga and Fayetteville shale samples analyzed by Bottoms (2017) have similar isotopic ratios.

9.3 Strontium Isotopes

The radioactive isotope of rubidium (^{87}Rb) decays to a stable isotope of strontium (^{87}Sr), which is used as a tracer to study geological processes and the geochemical evolution of the earth (Faure and Powell, 1972). The strontium distribution in rocks is largely controlled by its ability to substitute for Ca^{2+} in calcium-bearing minerals, as well as replacement of K^{+} in potassium feldspar (Faure and Powell, 1972). The isotopic composition of strontium in the oceans is thought to be uniform, but has changed throughout time and reflects input from different sources.

Faure and Powell (1972) suggested that seawater Sr reflects a balance between the weathering of young volcanics, which contributes lower Sr ratios ($^{87}Sr/^{86}Sr \sim 0.704$), while weathering of old granitic rocks contributes higher ratios ($^{87}Sr/^{86}Sr \sim 0.715$). Erosion of marine carbonate rocks contributes Sr that falls between these two values at $^{87}Sr/^{86}Sr \sim 0.708$ (Faure and Powell, 1972). Spooner (1976) proposed that unradiogenic Sr input was due to hydrothermal exchange with basaltic crust, which prompted many studies on the Sr flux and isotope composition of hydrothermal vents (Dickin, 2005). Palmer and Edmond (1989) measured the Sr budget and isotope ratios of major rivers and hydrothermal vent fluids and estimated global riverine flux to be 3.3×10^{10} mol Sr per year and $^{87}Sr/^{86}Sr \sim 0.7119$, while hydrothermal Sr flux was estimated to be half this magnitude and $^{87}Sr/^{86}Sr \sim 0.7035$. Two additional Sr inputs are the Sr released from diagenetic recrystallization of ocean-floor carbonates (Elderfield and Gieskes, 1982) and the run out of continental groundwater into the sea (Dickin, 2005). These competing Sr fluxes cause variations in the seawater Sr composition through time. The Boone chert samples analyzed in this study average $^{87}Sr/^{86}Sr \sim 0.708884$, which is comparable to the value Faure and Powell estimated for the erosion of marine carbonates. This value also agrees with the seawater Sr composition during the Mississippian (Figure 29), which is estimated to range from approximately 0.7075 to 0.7085 based on Sr isotope data collected from biogenic carbonates (Dickin, 2005). Biogenic carbonates are particularly reliable because they are fairly resistant to diagenetic alteration, and they are precipitated from seawater by organisms, so they do not contain a detrital fraction (Dickin, 2005). This whole rock chert samples from the Boone Formation analyzed in this study appear to reflect the Sr composition of seawater during the Mississippian. The effect of potential diagenetic alteration to the Sr isotopic composition of the cherts is unclear based on the available data. Within the Boone samples, there does not appear to be any systematic or stratigraphic variation in the radiogenic Sr content.

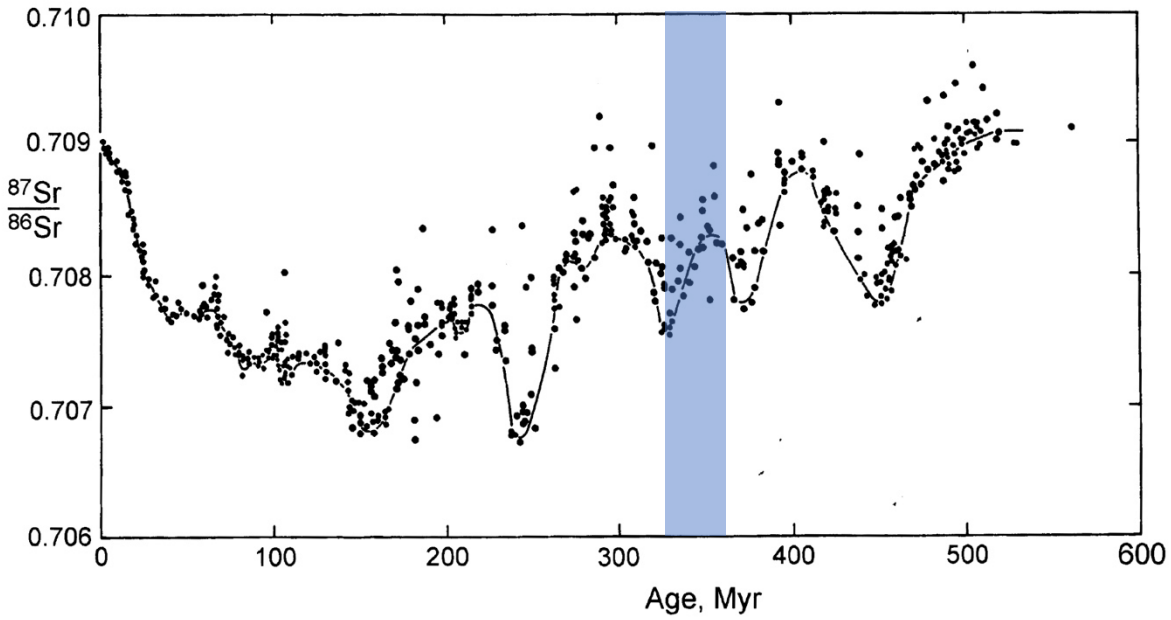

Figure 29. Sr isotope data for Phanerozoic carbonates. The solid line indicates the most probably sweater Sr composition. The blue highlighted interval represents the Mississippian. Figure from Dickin (2005) after Burke et al. (1982).

The Arkansas Novaculite contains Sr that is much more radiogenic (average $^{87}Sr/^{86}Sr \sim 0.7121$) in comparison to the Boone Formation. This could be explained by the much larger detrital component in the Arkansas Novaculite stratigraphic interval. While only siliceous novaculite was sampled for this study, the interval is interbedded with shales that likely supplied radiogenic Sr. XRD data for two Arkansas Novaculite samples indicates the presence of calcite and dolomite (~25%) within the siliceous novaculite samples, which may be susceptible to Sr substitution for Ca. The detrital component must have been sourced from old continental rocks containing very radiogenic Sr. The present day $^{87}Sr/^{86}Sr$ ratios of the Hatton Tuff samples are significantly higher than the Boone chert samples and the Arkansas Novaculite. Concentration data were not obtained for the Hatton Tuff samples, so these have not been age corrected for an accurate comparison with the Novaculite and Boone samples.

9.4 Neodymium Isotopes

Samarium and neodymium are light rare earth elements (LREE) inocrporated in many common rock-forming minerals. ^{143}Nd is a radiogenic isotope that forms from the decay of ^{147}Sm and is reported in reference to the stable isotope ^{144}Nd (Faure, 1977). The evolution of Nd in the earth is described by the chondritic uniform reservoir (CHUR) model, which assumes that terrestrial Nd evolved in a uniform reservoir, whose Sm/Nd ratio reflects that of chondritic meteorites (Faure, 1977). Using the present-day value of $^{143}Nd/^{144}Nd$ and the current Sm/Nd ratio, we can calculate the $^{143}Nd/^{144}Nd$ ratio of CHUR for any time in Earth's history (Faure, 1977). One useful way of comparing Nd isotope ratios of rocks of different ages is by calculating the deviation from the CHUR evolution line, which is expressed as epsilon (ε Nd) (Dickin, 2005; DePaolo and Wasserburg, 1976). Positive epsilon values indicate that the Nd in the rock came from "depleted" sources and negative epsilon values indicate an "enriched" source that had a lower Sm/Nd ratio than CHUR (Faure, 1977). All of the sedimentary rock samples analyzed for this study display negative epsilon values, implying dominantly an enriched source of Nd. The amount of variation in the epsilon values, however, may indicate the influence of different Nd sources. The Sm-Nd system is considered to be fairly resistant (relative to the Rb-Sr system) to alteration during chemical weathering, transport, deposition, and diagenesis of sedimentary rocks.

The $^{143}Nd/^{144}Nd$ ratios in seawater vary greatly within the ocean basin, but plot within quadrant IV (lower right) of the Nd-Sr diagram (Figure 27), which indicates that Nd ratios in seawater are largely controlled by continental inputs (Faure, 1977). Studies by Piepgras and Wasserburg showed that the $^{143}Nd/^{144}Nd$ ratios of the Atlantic Ocean are lower than the Pacific Ocean. They attributed this variation to the fact that the Atlantic Ocean is bordered by old rocks of sialic composition, while the Pacific Ocean is bordered by convergent margins, where

subduction induced volcanic activity produces high $^{143}Nd/^{144}Nd$ ratios (Faure, 1977; Piepgras and Wasserburg, 1980). Consequently, seawater Nd is controlled by the weathering of continents, but is affected by increased volcanic activity.

Calculated ε Nd values are presented in Figure 28. The Ordovician shales (Simbo, 2019), Chattanooga Shale (Bottoms, 2017), and Fayetteville Shale data (Bottoms, 2017), averaging -16.2, -17.0, and -12.5, respectively, are more negative than any of the chert samples, which average -5.5 for the entire Boone Formation. The upper Boone chert epsilon values are very similar to the measured Hatton Tuff (average ~ -3.75) which likely indicates that the rocks share the same silica source. The Novaculite displays more variation than the Boone cherts, but that could likely be explained by the fact that the Novaculite was deposited over a longer time with more potential for variation in source components than the Boone. The positive shift of epsilon values observed for the chert and tuff likely reflect the input of volcanogenic Nd from a depleted source. This effect was observed from Phanerozoic shales in France in a study by Michard et al. (1985), who observed positive shifts in epsilon values corresponding to orogenic periods, and the influx of volcanogenic detritus. Granite Mountain Syenite and Magnet Cove Carbonatite data are included in this plot to show what a purely igneous signature looks like for epsilon Nd, which is very different from the sedimentary Nd. No genetic relationship is suggested between these rocks and the sedimentary siliceous deposits. Shaw and Wasserburg (1985) analyzed Mississippian conodonts from carbonate rocks in Missouri and calculated epsilon values of -7.5, -7.1, -7.6, and -8.0. This is slightly more negative than the Boone cherts analyzed in this study, which average -5.5 for the entire Boone Formation. These values support the possibility that volcanogenic Nd was contributed to the chert.

10. CONCLUSIONS

Rare earth element concentrations normalized to MORB exhibit a negative trend, indicating that the cherts and novaculites are enriched in more incompatible elements rather than less incompatible elements relative to MORB. Normalized to average continental arcs, the upper Boone samples plot near 1, indicating similar compositions, while the lower Boone and Arkansas Novaculite have lower normalized values. A majority of the Boone chert samples display a negative Ce anomaly and a positive Y anomaly, which may indicate that they retain the seawater trace element concentrations from the time of their deposition. Much of the sampled chert from the Boone Formation contains radiogenic Pb isotope signatures that suggest a genetic relationship between the Boone Formation and the ores from the Northern Arkansas and Tri-State District MVT districts. Either the Boone Formation was a source of Pb in the ore deposits, or it assimilated radiogenic Pb during replacement of carbonate by silica via hydrothermal fluid alteration. Due to the low concentration of Pb in the Boone chert samples and the close stratigraphic proximity of the radiogenic Pb to the hydrothermally altered tripolitic chert interval, the latter interpretation is favored. The lowermost chert samples of the lower Boone and the uppermost chert samples of the upper Boone contain Pb that is less radiogenic than the tripolitic chert interval. The Sr isotope ratios for the Boone chert samples fall within the range of Sr isotope data collected from Lower Mississippian biogenic carbonates, which are used to estimate the Sr isotope composition of seawater. The Arkansas Novaculite contains Sr that is much more radiogenic and variable, which may indicate Sr exchange with the detrital component within the Arkansas Novaculite stratigraphic interval. Calculated ε Nd values for the rocks analyzed in this study are negative, indicating dominantly an enriched source of Nd. Positive shifts in ε Nd of the Boone Formation and some novaculites suggest the input of volcanogenic Nd during deposition. Similar ε Nd values for the upper Boone and Hatton Tuff suggest the same Nd source.

11. FUTURE RESEARCH

The limestone of the Boone Formation should also be examined to determine whether it has the same geochemical properties as its siliceous intervals. It is recommended that a broader geographic area be sampled to provide a better understanding of the distribution of radiogenic lead within the Mississippian chert-bearing carbonates. This would provide further insight into the extent of hydrothermal fluid alteration and potentially record the path that the fluids flowed. The Arkansas Novaculite should be examined at a higher resolution, with geochemical analysis of not only the novaculite component, but also the interbedded shales and chert. The Arkansas Novaculite is approximately 900 feet thick at the Caddo Gap exposure and warrants a higher resolution sampling frequency than was conducted in this study, in order to better identify stratigraphic trends and the geochemical signatures of the different lithologies within the stratigraphic interval. Only two Hatton Tuff samples were included in this study, but there are other major tuffs in the Ouachita Mountains that should be analyzed for isotopes and trace elements. These analyses would provide a better understanding of the volcanic component of the Mississippian rock record in the southern midcontinent region. In order to better constrain the silica source for the siliceous intervals, silicon isotopes should be utilized. It is recommended that the other siliceous intervals, especially the Ordovician cherts, within the Ozarks, Arkoma Basin, and Ouachita Mountains, should undergo geochemical analysis to establish an understanding of the isotope signatures of different chert intervals in this region. Silicon isotope analysis is also recommended for the abundant quartz veins that are present in the Ouachita Mountains region to better understand the silica source and mode of formation for these deposits. All of these geochemical data would collectively provide further insight into the tectonic history of the southern midcontinent region, seawater chemistry throughout the Paleozoic, and the diagenetic history of these rocks.

REFERENCES

Bottoms, B., 2017, A Geochemical Investigation and Comparison between Organic-rich Black Shales and Mississippi Valley-Type Pb-Zn ores in the Southern Ozarks Region, Unpublished Master of Science Thesis. University of Arkansas, 66 p.

Bottoms, B., Potra, A., Samuelsen, J.R., and Schutter, S.R., 2019, Geochemical investigations of the Woodford-Chattanooga and Fayetteville Shales: Implications for genesis of the Mississippi Valley-type zinc-lead ores in the southern Ozark Region and hydrocarbon exploration. AAPG Bulletin, in press.

Bradley, D. and Leach, D., 2003, Tectonic controls of Mississippi Valley-type lead–zinc mineralization in orogenic forelands. Mineralium Deposita, vol. 38, p. 652-667.

Brockie, D.C., Hare, E.H. Jr., Dingess, P.R., 1968, The geology and ore deposits of the Tri-State district of Missouri, Kansas, and Oklahoma. In Ridge JD (ed) Ore deposits of the United States, 1933-1967, v. 1, Graton-Sales v. American Institute of Mining, Matallurgical, and Petroleum Engineers, New York, p. 400-430.

Cains, J., Potra, A., & Pollock, E., 2016, Lower Mississippian Chert Development, Southern Midcontinent Region. Journal of the Arkansas Academy of Science, vol. 70, p. 59-63.

Chick, J., Cains, J., McFarlin, F., McKim, S., & Potra, A., 2017, Hydrothermally Emplaced, Lower Mississippian, Tripolitic Chert and Its Possible Relationship to the Tri-State Lead-Zinc Mining District. Journal of the Arkansas Academy of Science, vol. 71, p. 169-172.

Chinn, A. A., and Konig, R. H., 1973, Stress Inferred from Calcite Twin Lamellae in Relation to Regional Structure of Northwestern Arkansas. Geological Society of American Bulletin, v. 84, no. 11, p. 3731-3736.

Craig, H., Krishnaswami,S., and Somayajulu, B. L. K. 1973, ^{226}Pb-^{226}Ra: radioactive disequilibrium in the deep sea. Earth and Planetary Science Letters, v. 17, p. 295-305.

Cecil, C.B., 2004, Eolian Dust and the Origin of Sedimentary Chert. U. S. Geological Survey, Open-File Report 2004-1098, 13 p.

Cecil, C.B., 2015, Paleoclimate and the Origin of Paleozoic Chert: Time to Reexamine the Origins of Chert in the Rock Record. The Sedimentary Record, 13(3), p. 4-10.

De La Rocha, C.L., 2003, Silicon isotope fractionation by marine sponges and the reconstruction of the silicon isotope composition of ancient deep water. Geology, Geological Society of America, p. 423-426.

DePaolo, D.J., and Wasserburg, G.J., 1976, Inferences about magma sources and mantle structure from variations of ^{143}Nd/^{144}Nd. Geophysical Research Letters, v. 3, 743-746.

Dickin, A.P., 2005, Radiogenic Isotope Geology. Cambridge University Press, 492 p.

Diggs, W. E., 1961. Structural Framework of the Arkoma Basin. Tulsa Geological Society/Ft. Smith Geological Society, Field Trip Guidebook, April 14-15, 1961, p. 62-65.

Douthitt, C.B., 1982, The geochemistry of the stable isotopes of silicon. Geochimica et Cosmochimica Acta, v. 46, p. 1449–1458.

Elderfield, H. and Gieskes, J.M., 1982, Sr isotopes in insterstitial waters of marine sediments from Deep Sea Drilling Project cores. Nature, v. 300, p. 493-497.

Faure, G., 1986, Principles of Isotope Geology. 2nd edition, New York, New York: John Wiley & Sons, 589 p.

Faure, G., and Powell, J.L., 1972, Strontium Isotope Geology. Minerals, Rocks, and Inorganic Materials, v. 5, 171 p.

Flawn, P.T., Goldstein, A., King, P.B., Weaver, C.E., 1961, The Ouachita System. Publication-University of Texas, Bureau of Economic Geology, 401 p.

Goldstein A. 1959. Cherts and Novaculites of Ouachita Facies Oklahoma-Arkansas, and Texas. Special Publication – Society of Economic Paleontologists and Mineralogists v. 7, p. 135-149.

Griswold, L.S., 1892, Whetstones and the Novaculites of Arkansas. Annual Report of the Geological Survey of Arkansas for 1890, Press Printing Company, Little Rock, 443 p.

Groh, J., Bottoms, B., and Potra, A., 2017, Radiogenic Isotopes and Trace Element Constraints on the Source(s) and Evolution of Alkaline Igneous Rocks from Arkansas. 3rd UARC University of Arkansas Research Conference, November 11, 2017.

Guccione, M.J., 1993, Geologic history of Arkansas through time and space. Arkansas and Regional Studies Center, p.1-63.

Gutschick, R.C., and Sandberg, C.A., 1983, Mississippian Continental Margins of the Conterminous United States. In Stanley, D. J., and Moore, G. T., (eds.), The Shelfbreak: Critical Interface on Continental Margins. Society of Economic Paleontologists and Mineralogists, Special Publication 33, p. 79-86.

Harry, D.L., Mickus, K.L, 1998, Gravity constraints on lithosphere flexure and the structure of the late Paleozoic Ouachita orogen in Arkansas and Oklahoma, south central North America. Tectonics, v. 17, no. 2, p. 187-202.

Handford, C. R., and Manger, W. L., 1990. Sequence stratigraphy and sedimentology of the Mississippian System in northern Arkansas. Society of Economic Paleontologists and Mineralogists, Midcontinent Section, Guidebook, 64 p., pages unnumbered.

Hesse, R., 1990, Origin of Chert: Diagenesis of Biogenic Siliceous Sediments. In IA McIlreath, and DW Morrow, (eds.), Diagenesis, Geoscience Canada, Reprint Series v. 4, p. 227-251 (originally published in Geoscience Canada 15(3) September, 1988).

Houseknecht, D.W., and Matthews, S.M., 1985, Thermal Maturity of Carboniferous Strata, Ouachita Mountains. American Association of Petroleum Geologists Bulletin, v. 69, no. 3, p. 335-345.

Hudson, M., Cox, R., Cox, R.T., 2003, Late Paleozoic tectonics of the southern Ozark Dome. Repost of investigations – Tennessee Division of Geology, v. 51, p. 15-32.

Kastner, Miriam, Keene, J. B., and Gieskes, J. M., 1977. Diagenesis of Siliceous Oozes – 1, Chemical Controls on the Rate of Opal-A to Opal-CT Transition – An Experimental Study. Geochemica et Cosmochemica Acta, v. 412 (8), p. 1041-1051.

Keleman, P. B., Hanghoj, K., and Greene, A. R. 2004. One view of the geochemistry of subduction-related magmatic arcs, with an emphasis on primitive andesite and lower crust. Roberta L. Rudnick, H. D. Holland, and K. K. Turekian. Eds. Treatise on Geochemistry, v. 3, Elsevier, Oxford, 593-659.

Kesler, S.E., Martini, A.M., Appold, M.S., Walter, L.M., Huston, T.J., and Furman, F.C., 1996, Na-Cl-Br systematics of fluid inclusions from Mississippi Valley-Type deposits, Appalachian basin: constraints on solute origin and migration paths. Geochimica et Cosmochimica Acta, v. 60, p. 225-233.

Knauth, L.P., 1979, A model for the origin of chert in limestone. Geology, v. 7, p. 274-277.

Lane, H.R., 1978, The Burlington Shelf (Mississippian, North-central United States). Geologica et Palaeontologica, v. 12, p. 165-176.

Lane, H.R., and DeKeyser, T.L., 1980, Paleogeography of the Late Early Mississippian (Tournaisian 3) in the central and southwestern United States. Rocky Mountain Section, Society of Economic Paleontologists and Mineralogists, Paleontology Symposium 1, p. 149-162.

Leach, D.L., Bradley, D.C., Lewchuk, M.T., Symons, D.T.A., de Marsily, Ghislain, and Brannon, J.C., 2001, Mississippi Valley-Type lead-zinc deposits through geological time: implications from recent age-dating research: Mineralium Deposita, v. 36, p. 711–740.

Leach, D.L., and Sangster, D.F., 1993, Mississippi Valley- Type lead-zinc deposits. Geological Association of Canada Special Paper 40, p. 289–314.

Leach, D.L., Sangster, D.F., Kelley, K.D., Large, R.R., Garven, Grant, Allen, C.R., Gutzmer, Jens, and Walters, Steve, 2005, Sediment-hosted lead-zinc deposits: a global perspective. Society of Economic Geologists, Economic Geology One Hundredth Anniversary Volume, 1905–2005, p. 561–607.

Leach, D. L., Taylor, R. D., Fey, D. L., Diehl, S. F., and Saltus, R. W., 2010, A deposit model for Mississippi valley-type lead-zinc ores. Scientific Investigations Report, 52.

Liner, C. L., D. Zachry, and W. L. Manger. 2013. Mississippian characterization research in NW Arkansas. AAPG Mid-Continent Meeting, Wichita, KS.

Lowe, D.R., 1989, Pre-orogenic stratigraphy, sedimentology, and depositional setting, Ouachita Mountains. *In* R. D. Hatcher, The Geology of North America, Volume F-2, The Appalachian-Ouachita Orogen in the United States, Boulder, Colorado, The Geological Society of America, p. 575-590.

Manger, W.L., and Thompson, T.L., 1982, Regional Depositional Setting of Lower Mississippian Waulsortian Mound Facies, Southern Midcontinent, Arkansas, Missouri and Oklahoma. *In* Bolton, K., Lane, H.R., and LeMone, D.V., (eds.), Symposium on the Paleoenvironmental Setting and Distribution of the Waulsortian Facies, El Paso Geological Society and University of Texas at El Paso, p. 43-50.

Manger W.L., D.L. Zachry and W.L. Garrigan. 1988. An introduction to the geology of northwestern Arkansas: Field Trips. The Compass, Sigma Gamm Epsilon 65(4) p. 242-257.

McFarland, J.D., 1998 (revised 2004), Stratigraphic Summary of Arkansas. Arkansas Geological Commission, Information Circular 36, 39 p.

McFarlin, F.D., 2018, Stratigraphic Evaluation of the St. Joe-Boone Boundary Interval, Kinderhookian-Osagean Series, Lower Mississippian System, Tri-State Region, Southern Midcontinent. Unpublished Master of Science Thesis, 104 p.

McGilvery, T.A., Manger, W.L., and Zachry, D.L., 2016, Summary and Guidebook to the Depositional and Tectonic History of the Carboniferous Succession, Northwest Arkansas. Third Biennial Field Conference, AAPG Mid-Continent Section, 71 p.

McKim, S., 2018, The Origin of Tripolitic Chert and its Isotopic and Elemental Relationship to the Lead-Zinc Deposits in the Southern Ozark Region. Unpublished Undergraduate Honors Thesis, University of Arkansas, 34 p.

McKim, S., Cains, J., Chick, J., McFarlin, F., and Potra, A., 2017, Lithologic Stratigraphic Position, Sequence and Diagenetic History, Lower Mississippian Tripolitic Chert, Northern Arkansas and Southern Missouri. Journal of the Arkansas Academy of Science, v. 71, p. 165-168.

McKnight, E.T., 1935, Zinc and lead deposits of northern Arkansas. US Geological Survey Bulletin, no. 853.

Michard, A., Gurriet, P., Soudant, M., and Albarede, F., Nd isotpes in French Phanerozoic shales: external vs. internal aspects of crustal evolution. Geochimica et Cosmochimica Acta, v. 49, P. 601-610.

Minor, P. M., 2013. Analysis of tripolitic chert in the Boone Formation (lower Mississippian, Osagean), Northwest Arkansas and Southwestern Missouri. Unpublished Master of Science thesis, University of Arkansas, 80 p.

Miser, H. D. (1917). Manganese deposits of the Caddo Gap and DeQueen quadrangles, Arkansas. U.S. Geological Survey Bulletin 660-C, 59-122.

Miser, H.D., and Purdue, A.H., 1929, Geology of the McQueen and Caddo Gap quadrangles, Arkansas. U.S. Geological Survey Bulletin 808, p. 1-195.

Niem, A. R., 1971. Stratigraphy and Origin of Tuffs in the Stanley Group (Mississippian) Ouachita Flysch Basin, Oklahoma and Arkansas. Unpublished Ph.D. dissertation, University of Wisconsin, Madison, 151 p.

Niem, A. R., 1977. Mississippian Pyroclastic Flow and Ash-fall Deposits in the Deep-Marine Ouachita Flysch Basin, Oklahoma and Arkansas. Geological Society of America Bulletin, v. 88, p. 49-61.

Palmer, M.R., and Edmond, J.M., 1989, The strontium isotope budget of the modern ocean. Earth and Planetary Science Letters, v. 92, p. 11-26.

Park, D.E., 1961, The Origin of Bedded Silicates with Particular Reference to the Caballos and Arkansas Novaculite Formations. Unpublished Ph.D. Dissertation, Rice University, p. 80.

Philbrick, J.B.S., 2016, A Geochemical Analysis of the Arkansas Novaculite and Comparison to the Siliceous Deposits of the Boone Formation. Unpublished Master's Thesis, University of Arkansas, p. 1-60.

Piepgras, D.J. and Wasserburg, G.J, 1980, Neodymium isotopic variations in seawater. Earth and Planetary Science Letters, v. 50, p. 128-138.

Pin, C., Gannoun, A., and Dupont, A., 2014, Rapid, simultaneous separation of Sr, Pb, and Nd by extraction chromatography prior to isotope ratios determination by tims and mc-icp-ms. Journal of Analytical Atomic Spectrometry, v. 29, p. 1858-1870.

Potra, A., Garmin, W.T., Samuelsen, J.R., Wulff, A., and Pollock, E.D., 2018, Lead isotope trends and metal sources in the Mississippi Valley-type districts from the mid-continent United States. Journal of Geochemical Exploration, v. 192, p. 174-186.

Potra A., *Hardisty L., Philbrick J., and *Bottoms B., 2017, Isotope and trace element geochemistry of Cretaceous igneous rocks of the Arkansas Alkaline Province, USA: constraints on their origin and evolution. Goldschmidt Abstracts 3203.

Shaw, H.F. and Wasserburg, G.J., 1985, Sm-Nd in marine carbonates and phosphates: implications for Nd isotopes in seawater and crustal ages. Geochimica et Cosmochimica Acta, v. 49, p. 503-518.

Shelby, P. R., 1986. Depositional History of the St. Joe and Boone Formations in Northern Arkansas. Arkansas Academy of Science Proceedings, v. 40, p. 67-71.

Sholes, M., and McBride, E.F., 1975, Arkansas Novaculite *in* A Guidebook to the Sedimentology of Paleozoic Flysch and Associated Deposits, Ouachita Mountains - Arkoma Basin, Oklahoma, p. 69-87.

Simbo, C.W., 2019, The Paleozoic Sedimentary Rocks of the Ouachita Mountains and Arkoma Basin and their Genetic Relationship to the Mississippi Valley-Type Mineralization in the Southern Ozark Region: Insights from Radiogenic Pb Isotopes and Trace Elements Studies. Unpublished Master of Science Thesis, University of Arkansas, 66 p..

Stefurak, E.J.T., Fischer, W.W., and Lowe, D.R., 2015, Texture-specific Si isotope variations in Barberton Greenstone Belt cherts reord low temperature fractionations in early Archean seawater. Geochimica et Cosmochimica Acta 150, p. 26-52.

Tarr, W. A., 1926. The Origin of Chert and Flint. The University of Missouri Studies, v. 1, no. 2, 46 p., 10 pls.

Van den Boorn, S.H.J.M., Vroon, P.Z., van Belle, C.C., van der Wagt, B., Schwieters, J., and van Bergen, M.J., 2006, Determination of silicon isotope ratios in silicate materials by high-resolution MC-ICP-MS using a sodium hydroxide sample digestion method. Journal of Analytical Atomic Spectrometry, v. 21, p. 734-742.

Viets, J.G., Hofstra, A.H., Emsbo, Poul, and Kozlowski, Andrzej, 1996, The composition of fluid inclusions in ore and gangue minerals from Mississippi Valley-Type Zn-Pb deposits of the Cracow-Silesia region of southern Poland: genetic and environmental implications. In Gorecka, E., and Leach, D.L., eds., Carbonate-hosted zinc-lead deposits in the Silesian-Cracow area, Poland: Warsaw, Poland, Prace Panstwowego Instytuti Geologicznego, v. 154, p. 85–104.

Wenz, Z. J., M.S. Appold, K.L. Shelton, and S. Tesfaye. 2012. Geochemistry of Mississippi valley-type mineralizing fluids of the Ozark Plateau: A regional synthesis. American Journal of Science, v. 312, p. 22-80.

Wilson, J.L., and Majewske, O.P., 1960, Conjectured middle Paleozoic history of Central and West Texas. Aspects of the geology of Texas: a symposium: University of Texas Bulletin 6017, 117 p.

Zartman, R. E., and Doe, B. R., 1981, Plumbotectonics—the model. *Tectonophysics*, v. *75*, no. 1, p. 135-162.

Zimmerman, J., and Ford, J.T., 1988, Lower Stanley Shale and Arkansas Novaculite, western Mararn Basin and Caddo Gap, Ouachita Mountains, Arkansas. Centennial Field Guide - South Central Section, Geological Society of America, p. 267-272.

APPENDICES

Appendix 1.1 Sample Descriptions

Lab Label	Outcrop Label	Outcrop Location	Formation	Member
J1	BV1	Bella Vista, AR	Boone	Upper Boone
J2	BV3	Bella Vista, AR	Boone	Upper Boone
J3	BV5	Bella Vista, AR	Boone	Upper Boone
J4	BV7	Bella Vista, AR	Boone	Upper Boone
J5	BV9	Bella Vista, AR	Boone	Upper Boone
J6	BV11	Bella Vista, AR	Boone	Upper Boone
J7	BV14	Bella Vista, AR	Boone	Upper Boone
J8	P2	Pineville, MO	Boone	Lower Boone
J9	P3	Pineville, MO	Boone	Lower Boone
J10	P4	Pineville, MO	Boone	Lower Boone
J11	P5	Pineville, MO	Boone	Lower Boone
J12	P7	Pineville, MO	Boone	Lower Boone
J13	P8	Pineville, MO	Boone	Lower Boone
J14	P10	Pineville, MO	Boone	Lower Boone
J15	P12	Pineville, MO	Boone	Lower Boone
J16	P14	Pineville, MO	Boone	Upper Boone
J17	P16	Pineville, MO	Boone	Upper Boone
J18	K1	Kansas, OK	Boone	Lower Boone
J19	BAP	Branson Airport, MO	St. Joe	Pierson
J20	K3	Kansas, OK	Boone	Lower Boone
J21	K4	Kansas, OK	Boone	Lower Boone
J22	HT4	Hatton, AR	Stanley	Hatton Tuff
J23	HT5	Hatton, AR	Stanley	Hatton Tuff
J30	Pit1	Deer, AR	Pitkin	Pitkin
J31	CG6	Caddo Gap, AR	Arkansas Novaculite	Lower Novaculite
J32	CG8	Caddo Gap, AR	Arkansas Novaculite	Lower Novaculite
J33	CG18	Caddo Gap, AR	Arkansas Novaculite	Lower Novaculite
J34	CG39	Caddo Gap, AR	Arkansas Novaculite	Lower Novaculite
J35	CG52	Caddo Gap, AR	Arkansas Novaculite	Lower Novaculite
J36	CG71	Caddo Gap, AR	Arkansas Novaculite	Upper Novaculite
J37	CG77	Caddo Gap, AR	Arkansas Novaculite	Upper Novaculite
J38	CG82	Caddo Gap, AR	Arkansas Novaculite	Upper Novaculite
J39	CG85	Caddo Gap, AR	Arkansas Novaculite	Upper Novaculite
J40	CG86	Caddo Gap, AR	Arkansas Novaculite	Upper Novaculite

Appendix 2.1. Trace Element Concentrations (ppm)

Sample	Li	Be	Sc	V	Cr	Co	Ni	Cu	Zn	Ga	As	Rb	Sr	Y	Zr	Nb	Sb	Cs	Ba
BAP	6.969	0.078	0.850	2.702	1.586	1.848	3.939	0.504	9.568	0.493	2.373	3.062	33.877	3.762	2.465	0.251	0.268	0.245	19.076
BV1	0.322	0.017	0.852	2.129	3.525	0.218	1.850	0.280	18.529	0.869	1.549	0.888	79.503	11.410	0.518	0.066	0.013	0.092	5.295
BV3	1.929	0.086	10.313	13.618	13.500	0.348	3.371	0.430	180.497	2.949	1.628	4.928	353.120	89.946	1.779	0.269	0.012	0.316	9.152
BV3r*	3.101	0.126	28.649	23.255	19.588	0.564	4.130	0.465	294.437	4.214	2.475	18.579	1234.161	213.771	3.065	0.394	0.023	0.816	18.780
BV5	1.339	0.097	7.209	12.768	17.588	0.213	1.307	0.229	32.270	2.157	1.179	5.004	527.513	71.243	1.310	0.155	0.016	0.304	13.432
BV7	1.752	0.086	10.812	13.206	17.885	0.369	1.315	0.196	56.208	3.314	1.844	11.300	1080.116	117.213	3.115	0.248	0.023	0.488	15.914
BV9	1.394	0.063	5.549	20.221	13.766	0.127	1.551	0.414	32.864	2.804	1.918	9.304	509.009	92.697	2.262	0.211	0.030	0.447	29.211
BV11	1.716	0.029	7.098	7.765	7.854	0.636	1.306	0.265	13.849	2.032	1.099	11.398	1481.903	79.173	1.780	0.248	0.019	0.478	17.494
BV14	2.388	0.034	6.007	12.441	8.495	0.523	1.585	0.595	19.151	3.411	1.174	18.939	1083.214	79.022	3.317	0.369	0.030	0.728	33.840
P2	11.701	0.097	9.819	21.374	10.609	2.871	10.315	2.407	31.042	4.698	2.948	57.054	507.116	22.473	9.033	0.995	0.055	2.997	79.135
P3	10.925	0.194	18.976	33.960	14.638	2.564	9.287	1.344	6.937	6.500	7.626	73.872	3982.179	64.611	10.994	1.182	0.136	3.354	72.635
P5	24.098	0.429	23.267	63.127	40.246	3.881	15.162	5.264	97.010	17.741	14.532	163.056	496.646	25.556	22.599	2.321	0.200	7.221	155.495
P7	38.082	0.680	30.051	82.210	44.846	4.514	25.266	7.342	66.285	18.164	17.249	262.358	2486.717	75.418	30.780	3.023	0.240	12.626	383.628
P8	9.876	0.206	5.769	23.706	11.034	1.045	6.092	1.204	55.259	5.039	17.775	65.821	603.836	20.547	8.969	0.651	0.050	3.437	123.620
P10	9.249	0.257	5.155	11.259	8.757	1.253	6.098	0.958	17.357	5.605	3.079	50.931	717.255	9.428	7.160	0.611	0.067	3.007	59.857
P12	6.865	0.154	11.301	17.085	8.990	1.117	4.191	0.890	7.371	4.445	2.522	43.751	2030.896	40.141	5.712	0.505	0.029	2.081	65.229
P14	5.848	0.114	3.854	10.195	4.813	0.662	3.202	0.637	26.300	3.590	3.556	36.660	778.075	12.661	4.324	0.386	0.015	1.656	54.973
P16	3.700	0.171	31.374	15.707	9.486	0.852	3.540	0.736	33.805	3.262	4.860	21.387	2437.665	157.233	2.224	0.213	0.025	0.687	14.666
K1	5.771	0.109	0.544	15.677	2.187	3.758	38.617	2.064	2.660	0.395	0.960	2.483	26.951	3.405	3.114	0.708	0.052	0.200	35.997
K1d*	7.740	0.138	0.670	17.629	2.054	4.250	43.207	2.103	3.315	0.450	1.136	3.216	30.750	3.730	3.313	0.727	0.055	0.215	36.842
K3	10.564	0.248	1.186	13.386	6.480	0.957	11.192	1.706	2.077	1.061	1.013	7.694	29.916	4.535	5.173	0.517	0.042	0.460	27.491
K4	2.242	0.059	0.271	4.103	2.292	0.455	3.051	1.022	0.568	0.280	0.857	1.586	4.027	1.411	1.318	0.110	0.019	0.087	8.053
Pit1	29.673	0.276	1.783	10.697	29.439	0.844	5.213	2.316	26.561	1.613	1.894	9.447	240.740	11.150	10.596	0.879	0.050	0.500	95.560
CG6	10.278	0.381	4.081	9.071	4.929	2.748	6.043	17.451	7.746	3.937	0.284	19.200	31.177	7.915	17.154	1.026	0.073	1.552	112.547
CG8	3.037	0.104	1.532	7.476	2.337	0.115	0.565	0.864	0.667	0.964	0.379	5.877	16.445	1.486	7.842	0.486	0.034	0.426	56.178
CG18	6.539	0.034	0.934	3.056	1.088	21.728	5.364	22.191	3.342	0.324	0.104	1.670	11.883	3.112	7.799	0.190	0.006	0.096	20.550
CG39	2.055	0.031	0.738	3.276	1.472	0.014	0.545	0.335	0.523	0.408	0.048	2.479	9.810	9.106	5.686	0.169	0.006	0.128	16.845
CG52	3.048	0.656	2.260	113.503	10.456	0.270	14.145	33.539	1.824	2.996	5.295	11.826	35.625	6.337	16.894	1.020	0.659	0.746	100.571
CG71	2.623	0.147	0.923	38.081	9.012	1.861	8.217	9.896	46.562	0.867	4.368	5.484	23.557	2.954	5.219	0.312	0.400	0.544	302.759
CG77	8.294	0.060	1.775	1.555	1.784	0.056	0.369	1.201	0.382	0.395	0.116	0.305	0.667	36.571	0.727	0.025	0.035	0.019	3.911
CG82	1.766	0.070	0.471	2.666	1.127	0.083	0.374	3.748	2.346	0.361	0.182	2.064	7.759	3.010	1.157	0.057	0.030	0.183	37.761
CG85	18.520	0.048	0.606	1.223	0.882	0.143	0.937	1.740	1.146	0.394	0.129	0.264	1.791	6.820	0.419	0.028	0.032	0.032	7.315
CG86	22.294	0.135	1.339	10.288	4.398	1.833	4.923	6.303	26.789	1.670	0.440	11.438	31.044	4.899	5.983	0.432	0.038	0.629	144.548

Appendix 2.1 Trace Element Concentrations (continued)

Sample	La	Ce	Pr	Nd	Sm	Eu	Gd	Tb	Dy	Ho	Er	Tm	Yb	Lu	Ta	Tl	Pb	Th	U
BAP	2.233	2.524	0.561	2.377	0.473	0.111	0.519	0.076	0.400	0.080	0.216	0.025	0.157	0.024	0.015	0.010	3.070	0.185	0.419
BV1	3.621	2.967	0.914	3.667	0.733	0.154	0.518	0.105	0.636	0.127	0.323	0.038	0.195	0.050	0.003	0.006	0.656	0.151	0.227
BV3	16.952	12.871	5.028	21.324	4.803	0.989	3.342	0.647	3.697	0.702	1.695	0.180	0.914	0.259	0.012	0.015	4.976	0.536	0.768
BV3r*	25.872	16.766	7.666	30.837	6.837	1.346	3.534	0.769	4.294	0.791	1.868	0.189	0.964	0.418	0.013	0.014	4.724	0.521	0.701
BV5	16.188	10.064	4.013	15.457	3.250	0.707	1.982	0.418	2.473	0.503	1.291	0.150	0.807	0.263	0.007	0.010	0.944	0.400	0.418
BV7	27.710	13.807	6.070	23.222	4.675	1.071	2.651	0.555	3.341	0.671	1.751	0.199	1.064	0.368	0.013	0.010	0.676	0.431	0.632
BV9	19.292	8.118	4.987	20.804	4.447	0.895	2.536	0.489	2.818	0.527	1.250	0.126	0.635	0.236	0.010	0.015	0.958	0.234	1.521
BV11	17.075	5.811	3.582	13.622	2.635	0.526	1.376	0.282	1.668	0.341	0.914	0.100	0.530	0.214	0.017	0.011	0.417	0.128	0.197
BV14	19.673	9.829	4.459	16.627	3.245	0.656	1.584	0.328	1.859	0.359	0.920	0.102	0.530	0.219	0.012	0.016	0.394	0.217	0.261
P2	6.310	5.446	1.669	6.270	1.270	0.242	0.571	0.122	0.652	0.124	0.310	0.037	0.200	0.095	0.030	0.037	2.704	0.365	0.322
P3	12.819	9.501	3.309	12.454	2.517	0.501	1.160	0.241	1.322	0.248	0.630	0.068	0.365	0.172	0.032	0.033	2.296	0.373	0.441
P5	8.775	7.238	2.148	7.495	1.455	0.252	0.566	0.120	0.643	0.123	0.330	0.040	0.234	0.121	0.060	0.070	4.513	0.823	0.465
P7	15.542	12.354	4.492	17.134	3.533	0.706	1.532	0.302	1.596	0.286	0.718	0.076	0.428	0.219	0.040	0.286	9.664	1.068	1.063
P8	4.055	3.046	1.129	4.313	0.919	0.183	0.388	0.080	0.406	0.073	0.177	0.018	0.096	0.051	0.016	0.112	1.934	0.248	0.241
P10	2.278	1.567	0.544	1.931	0.377	0.077	0.167	0.035	0.187	0.035	0.092	0.011	0.063	0.034	0.013	0.069	1.850	0.228	0.337
P12	6.133	4.122	1.617	6.115	1.255	0.247	0.562	0.122	0.673	0.125	0.314	0.033	0.182	0.092	0.011	0.026	0.868	0.220	0.220
P14	2.319	1.555	0.574	2.113	0.426	0.085	0.183	0.038	0.208	0.038	0.098	0.010	0.057	0.030	0.008	0.045	0.646	0.105	0.118
P16	22.699	12.673	5.557	20.058	3.922	0.764	1.825	0.394	2.234	0.413	1.015	0.108	0.560	0.281	0.007	0.015	0.518	0.175	0.221
K1	1.535	5.434	0.429	1.917	0.438	0.113	0.506	0.079	0.433	0.088	0.251	0.033	0.195	0.030	0.013	0.359	1.261	0.276	0.136
K1d*	1.579	5.551	0.441	2.000	0.460	0.116	0.537	0.081	0.444	0.090	0.254	0.031	0.197	0.030	0.013	0.422	1.309	0.284	0.140
K3	3.640	4.230	0.915	3.770	0.722	0.155	0.741	0.108	0.576	0.117	0.338	0.043	0.269	0.041	0.038	0.132	3.264	0.500	0.522
K4	1.115	1.517	0.284	1.182	0.230	0.050	0.233	0.034	0.181	0.037	0.106	0.013	0.079	0.012	0.008	0.035	1.554	0.147	0.171
Pit1	6.230	8.147	1.507	6.256	1.226	0.324	1.364	0.205	1.145	0.248	0.742	0.094	0.589	0.092	0.072	0.070	1.454	1.152	1.180
CG6	5.905	16.614	1.811	7.710	1.823	0.431	1.934	0.284	1.460	0.270	0.757	0.096	0.631	0.099	0.084	0.065	3.431	1.473	0.375
CG8	1.571	4.332	0.431	1.687	0.367	0.103	0.392	0.058	0.294	0.055	0.160	0.023	0.174	0.029	0.035	0.027	1.349	0.594	0.256
CG18	4.932	5.380	1.167	4.847	0.913	0.196	0.883	0.123	0.597	0.107	0.285	0.034	0.225	0.032	0.014	0.025	0.517	0.464	0.201
CG39	2.877	2.590	0.635	2.646	0.572	0.144	0.741	0.138	0.879	0.212	0.664	0.092	0.600	0.092	0.014	0.016	0.097	0.366	0.201
CG52	3.658	6.345	1.119	4.687	1.125	0.291	1.208	0.188	1.057	0.219	0.684	0.100	0.780	0.127	0.054	0.286	2.973	0.724	2.820
CG71	1.463	3.321	0.395	1.630	0.374	0.198	0.457	0.066	0.394	0.083	0.256	0.035	0.261	0.045	0.021	0.155	1.072	0.341	3.310
CG77	0.334	0.352	0.171	1.286	0.834	0.299	1.859	0.443	3.377	0.792	2.224	0.276	1.632	0.223	0.008	0.001	0.027	0.132	0.265
CG82	1.169	2.143	0.315	1.324	0.295	0.086	0.386	0.063	0.344	0.067	0.182	0.022	0.133	0.020	0.004	0.017	1.012	0.109	0.324
CG85	3.444	3.892	1.150	5.489	1.256	0.267	1.110	0.165	0.813	0.160	0.455	0.055	0.341	0.048	0.003	0.000	0.227	0.213	0.129
CG86	4.767	10.057	1.341	5.733	1.350	0.351	1.445	0.200	0.918	0.156	0.394	0.044	0.297	0.047	0.032	0.050	1.598	0.668	0.191

Appendix 3.1 Detailed Isotope Data

Outcrop Label	Formation/Member	$^{208}Pb/^{204}Pb$	error	$^{207}Pb/^{204}Pb$	error	$^{206}Pb/^{204}Pb$	error	$^{87/86}Sr$	error	$^{143/144}Nd$	error
BAP	St Joe: Pierson	38.7455	{ 4.99E-04 }	15.6871	{ 1.73E-04 }	19.2449	{ 2.04E-04 }	0.710304	{ 5.84E-06 }	0.512197	{ 3.10E-06 }
P2	Lower Boone	39.7230	{ 5.85E-04 }	15.7851	{ 2.23E-04 }	20.4621	{ 2.75E-04 }	0.711023	{ 6.01E-06 }	0.512152	{ 3.58E-06 }
P3	Lower Boone	39.6222	{ 6.69E-04 }	15.7905	{ 2.34E-04 }	20.4977	{ 2.80E-04 }	0.708212	{ 5.35E-06 }	0.512185	{ 3.34E-06 }
P4	Lower Boone	39.6771	{ 6.87E-04 }	15.7838	{ 2.72E-04 }	20.4691	{ 3.00E-04 }	0.711020	{ 5.65E-06 }	0.512135	{ 5.50E-06 }
P5	Lower Boone	39.7233	{ 7.15E-04 }	15.7809	{ 2.48E-04 }	20.4137	{ 3.04E-04 }	0.714478	{ 6.00E-06 }	0.512105	{ 3.49E-06 }
P7	Lower Boone	40.1589	{ 6.11E-04 }	15.8384	{ 2.35E-04 }	21.0689	{ 2.75E-04 }	0.710492	{ 5.53E-06 }	0.512146	{ 4.35E-06 }
P7	Lower Boone	40.1493	{ 5.24E-04 }	15.8350	{ 2.27E-04 }	21.0714	{ 2.49E-04 }	0.710519	{ 6.37E-06 }	0.512152	{ 3.58E-06 }
P8	Lower Boone	40.1464	{ 8.63E-04 }	15.8372	{ 2.96E-04 }	21.2575	{ 3.24E-04 }	0.710546	{ 6.21E-06 }	0.512161	{ 5.18E-06 }
P10	Lower Boone	40.1156	{ 5.00E-04 }	15.8429	{ 2.04E-04 }	21.3028	{ 2.97E-04 }	0.709748	{ 4.19E-06 }	0.512177	{ 8.24E-06 }
P12	Lower Boone	40.0721	{ 7.00E-04 }	15.8428	{ 2.43E-04 }	21.2658	{ 2.91E-04 }	0.708290	{ 5.81E-06 }	0.512187	{ 3.34E-06 }
K1	Lower Boone	38.6232	{ 7.22E-04 }	15.6599	{ 2.64E-04 }	18.8345	{ 2.95E-04 }	0.710988	{ 5.36E-06 }	0.512202	{ 3.91E-06 }
K3	Lower Boone	38.8602	{ 7.16E-04 }	15.7071	{ 2.74E-04 }	19.5607	{ 3.36E-04 }	0.712938	{ 5.22E-06 }	0.512158	{ 3.34E-06 }
K4	Lower Boone	39.1076	{ 5.63E-04 }	15.7538	{ 2.05E-04 }	20.3320	{ 2.50E-04 }	0.714981	{ 6.01E-06 }	0.512156	{ 5.79E-06 }
BV1	Upper Boone	40.1788	{ 7.05E-04 }	15.8970	{ 2.63E-04 }	22.2969	{ 3.48E-04 }	0.709098	{ 4.76E-06 }	0.512191	{ 4.19E-06 }
BV3	Upper Boone	40.4346	{ 5.78E-04 }	15.8959	{ 2.26E-04 }	21.9110	{ 2.82E-04 }	0.708867	{ 5.86E-06 }	0.509752	{ 1.27E-03 }
BV5	Upper Boone	40.3212	{ 8.41E-04 }	15.9390	{ 3.19E-04 }	22.9937	{ 4.70E-04 }	0.708916	{ 5.90E-06 }	0.512257	{ 3.08E-06 }
BV7	Upper Boone	40.0450	{ 7.18E-04 }	15.8994	{ 2.49E-04 }	22.6978	{ 3.32E-04 }			0.512225	{ 2.43E-05 }
BV11	Upper Boone	39.4391	{ 6.56E-04 }	15.7962	{ 2.32E-04 }	21.0044	{ 2.90E-04 }	0.708727	{ 6.31E-06 }	0.510181	{ 3.56E-03 }
BV14	Upper Boone	39.6893	{ 1.43E-03 }	15.8271	{ 5.56E-04 }	21.6243	{ 7.97E-04 }	0.709322	{ 5.53E-06 }	0.512271	{ 4.66E-06 }
P14	Elsey	40.0391	{ 7.98E-04 }	15.8379	{ 2.84E-04 }	21.3534	{ 4.38E-04 }	0.708822	{ 5.28E-06 }	0.512179	{ 7.05E-06 }
P16	Elsey	40.2242	{ 8.97E-04 }	15.8643	{ 3.17E-04 }	21.7211	{ 4.50E-04 }	0.709014	{ 5.39E-06 }	0.512223	{ 3.49E-06 }
Pit1	Pitkin	39.2772	{ 2.31E-03 }	15.8259	{ 9.56E-04 }	21.6314	{ 1.33E-03 }	0.708739	{ 5.30E-06 }	0.512098	{ 3.56E-06 }
HT4	Hatton Tuff	39.1791	{ 5.98E-04 }	15.6687	{ 2.39E-04 }	19.0531	{ 2.72E-04 }	0.737447	{ 6.62E-06 }	0.512264	{ 6.00E-06 }
HT5	Hatton Tuff	40.0042	{ 5.72E-04 }	15.6904	{ 1.79E-04 }	19.5468	{ 2.30E-04 }	0.736163	{ 5.95E-06 }	0.512238	{ 8.16E-06 }
CG6	Lower Novaculite	38.9604	{ 5.90E-04 }	15.6607	{ 2.02E-04 }	18.7759	{ 2.22E-04 }	0.724588	{ 5.94E-06 }	0.512022	{ 2.96E-06 }
CG8	Lower Novaculite	38.9528	{ 6.46E-04 }	15.6768	{ 2.35E-04 }	19.0813	{ 2.69E-04 }	0.719874	{ 5.55E-06 }	0.512001	{ 5.57E-06 }
CG18	Lower Novaculite	39.6727	{ 8.80E-04 }	15.7861	{ 3.51E-04 }	20.8876	{ 4.21E-04 }	0.714738	{ 4.67E-06 }	0.512035	{ 3.05E-06 }
CG39	Lower Novaculite	42.4587	{ 2.31E-03 }	15.9955	{ 9.16E-04 }	25.1670	{ 1.43E-03 }	0.717184	{ 5.46E-06 }	0.512041	{ 3.28E-06 }
CG52	Lower Novaculite	38.6416	{ 5.82E-04 }	15.8793	{ 2.31E-04 }	22.6982	{ 3.18E-04 }	0.716938	{ 3.70E-06 }	0.512180	{ 5.66E-06 }
CG71	Upper Novaculite	38.7656	{ 6.30E-04 }	16.2598	{ 2.71E-04 }	29.5943	{ 4.62E-04 }	0.714945	{ 6.70E-06 }	0.512090	{ 3.11E-06 }
CG77	Upper Novaculite	39.3755	{ 5.82E-03 }	15.9556	{ 2.31E-03 }	24.8650	{ 3.83E-03 }	0.712124	{ 6.15E-06 }	0.512159	{ 4.67E-06 }
CG82	Upper Novaculite	38.6353	{ 6.86E-04 }	15.7689	{ 2.50E-04 }	20.7863	{ 3.89E-04 }	0.715391	{ 4.15E-06 }	0.512221	{ 4.34E-06 }
CG85	Upper Novaculite	39.2452	{ 1.32E-03 }	15.7989	{ 5.24E-04 }	21.5355	{ 6.89E-04 }	0.713192	{ 6.09E-06 }	0.512198	{ 3.11E-06 }
CG86	Upper Novaculite	38.8443	{ 7.51E-04 }	15.6671	{ 2.83E-04 }	18.9189	{ 3.08E-04 }	0.717451	{ 5.65E-06 }	0.512230	{ 5.99E-06 }

Appendix 3.2. Pb Standard Analyses

Standard	$^{208}Pb/^{204}Pb$	error	$^{207}Pb/^{204}Pb$	error	$^{206}Pb/^{204}Pb$	error
NBS 981	36.667	{ 6.72E-04 }	15.481	{ 2.68E-04 }	16.929	{ 2.64E-04 }
NBS 981	36.667	{ 4.92E-04 }	15.482	{ 1.77E-04 }	16.929	{ 2.08E-04 }
NBS 981	36.667	{ 6.26E-04 }	15.482	{ 2.62E-04 }	16.929	{ 2.66E-04 }
NBS 981	36.666	{ 4.72E-04 }	15.481	{ 1.93E-04 }	16.929	{ 2.08E-04 }
NBS 981	36.666	{ 5.81E-04 }	15.481	{ 2.24E-04 }	16.929	{ 2.46E-04 }
NBS 981	36.666	{ 5.55E-04 }	15.482	{ 2.05E-04 }	16.929	{ 1.83E-04 }
NBS 981	36.666	{ 4.84E-04 }	15.481	{ 1.95E-04 }	16.928	{ 2.17E-04 }
NBS 981	36.667	{ 5.21E-04 }	15.482	{ 2.08E-04 }	16.929	{ 1.98E-04 }
NBS 981	36.665	{ 4.73E-04 }	15.481	{ 1.90E-04 }	16.928	{ 1.97E-04 }
NBS 981	36.668	{ 6.17E-04 }	15.482	{ 2.48E-04 }	16.929	{ 2.48E-04 }
NBS 981	36.626	{ 6.27E-04 }	15.469	{ 2.45E-04 }	16.919	{ 2.15E-04 }
NBS 981	36.635	{ 5.16E-04 }	15.471	{ 1.90E-04 }	16.921	{ 1.88E-04 }
NBS 981	36.634	{ 4.84E-04 }	15.471	{ 1.62E-04 }	16.921	{ 1.92E-04 }
NBS 981	36.634	{ 5.90E-04 }	15.471	{ 2.17E-04 }	16.921	{ 1.93E-04 }
NBS 981	36.634	{ 4.86E-04 }	15.471	{ 1.81E-04 }	16.921	{ 1.89E-04 }
NBS 981	36.631	{ 5.95E-04 }	15.470	{ 2.10E-04 }	16.920	{ 1.96E-04 }
Average	36.654		15.477		16.926	
Todt et al. 1996	36.701		15.485		16.936	

Appendix 3.3 Nd and Sr Standard Analyses

Standard	$^{143}Nd/^{144}Nd$	error	Standard	$^{87}Sr/^{86}Sr$	error
JNdi	0.51206	{ 2.56E-06 }	SRM 987	0.71020	{ 5.23E-06 }
JNdi	0.51206	{ 3.21E-06 }	SRM 987	0.71021	{ 4.71E-06 }
JNdi	0.51205	{ 3.66E-06 }	SRM 987	0.71022	{ 5.75E-06 }
JNdi	0.51205	{ 2.62E-06 }	SRM 987	0.71023	{ 5.60E-06 }
JNdi	0.51205	{ 3.70E-06 }	SRM 987	0.71022	{ 5.62E-06 }
JNdi	0.51205	{ 3.89E-06 }	SRM 987	0.71022	{ 5.78E-06 }
JNdi	0.51205	{ 3.96E-06 }	SRM 987	0.71023	{ 7.13E-06 }
JNdi	0.51205	{ 3.41E-06 }	SRM 987	0.71021	{ 6.87E-06 }
JNdi	0.51205	{ 3.66E-06 }	SRM 987	0.71020	{ 6.28E-06 }
JNdi	0.51205	{ 3.41E-06 }	SRM 987	0.71022	{ 5.52E-06 }
JNdi	0.51204	{ 3.00E-06 }	SRM 987	0.71024	{ 5.77E-06 }
JNdi	0.51204	{ 2.91E-06 }	SRM 987	0.71020	{ 5.30E-06 }
JNdi	0.51205	{ 3.57E-06 }	SRM 987	0.71023	{ 4.80E-06 }
JNdi	0.51205	{ 3.93E-06 }	SRM 987	0.71023	{ 4.46E-06 }
JNdi	0.51205	{ 2.95E-06 }	SRM 987	0.71022	{ 5.33E-06 }
JNdi	0.51205	{ 3.43E-06 }	SRM 987	0.71016	{ 5.51E-06 }
JNdi	0.51205	{ 3.17E-06 }	SRM 987	0.71022	{ 5.33E-06 }
JNdi	0.51204	{ 3.69E-06 }	SRM 987	0.71022	{ 6.87E-06 }
JNdi	0.51205	{ 3.34E-06 }	SRM 987	0.71023	{ 4.69E-06 }
Average	0.51205		**Average**	0.71022	
Tanaka et al., 2000	0.51212		SRM 987	0.71026	

Appendix 3.4 εNd

Formation/Member	Sample	Approximate Age (Ma)	E Nd (t)
St Joe: Pierson	BAP	355.0	-5.17
Lower Boone	P2	350.0	-6.15
Lower Boone	P3	350.0	-5.48
Lower Boone	P4	350.0	-6.84
Lower Boone	P5	350.0	-6.36
Lower Boone	P7	350.0	-6.25
Lower Boone	P8	350.0	-5.46
Lower Boone	P12	350.0	-5.54
Lower Boone	K1	350.0	-5.86
Lower Boone	K3	350.0	-5.72
Lower Boone	K4	350.0	-5.85
Upper Boone	BV1	350.0	-5.30
Upper Boone	BV5	350.0	-4.31
Upper Boone	BV7	350.0	-4.68
Upper Boone	BV14	350.0	-3.62
Upper Boone/Elsey	P14	350.0	-5.58
Upper Boone/Elsey	P16	350.0	-4.57
Pitkin	Pit1	325.0	-6.65
Lower Novaculite	CG6	360.0	-9.59
Lower Novaculite	CG8	360.0	-9.50
Lower Novaculite	CG18	360.0	-8.05
Lower Novaculite	CG39	360.0	-8.67
Lower Novaculite	CG52	360.0	-6.60
Upper Novaculite	CG71	350.0	-8.08
Upper Novaculite	CG77	350.0	-18.01
Upper Novaculite	CG82	350.0	-5.33
Upper Novaculite	CG85	350.0	-5.95
Upper Novaculite	CG86	350.0	-5.51

Appendix 3.4 εNd (continued)

Formation/Member	Sample	Approximate Age (Ma)	E Nd (t)
Fayetteville Shale	FS7L	325.0	-8.75
Fayetteville Shale	FS10L	325.0	-13.31
Fayetteville Shale	FS8UU	360.0	-15.46
Chattanooga Shale	CS9	360.0	-17.81
Chattanooga Shale	CS12	360.0	-16.89
Chattanooga Shale	CS12d	360.0	-16.30
Magnet Cove	MC2	100.0	3.13
Magnet Cove	MC8	100.0	3.08
Magnet Cove	MC3	100.0	3.53
Magnet Cove	MC 9	100.0	1.42
Magnet Cove	MC 7	100.0	3.76
Granite Mountain Syenite	GM11	100.0	1.32
Granite Mountain Syenite	GM 6	100.0	2.71
Granite Mountain Syenite	GM 8	100.0	2.19
Granite Mountain Syenite	GM5	100.0	1.04
Granite Mountain Syenite	GM 10	100.0	1.79
Granite Mountain Syenite	GM 12	100.0	1.34
Granite Mountain Syenite	GM9	100.0	0.80
Hatton Tuff	HT4	325.0	-3.50
Hatton Tuff	HT5	325.0	-4.01
Jackfork Sandstone	UJ2 SS	325.0	-12.38
Jackfork Sandstone	LJ-1	325.0	7.78
Womble Shale	Womble 2	450.0	-21.06
Mazarn Shale	Mazarn 2	450.0	-23.11
Mazarn Shale	Mazarn 5	450.0	-9.72
Mazarn Shale	Mazarn 3	450.0	-10.98

Appendix 4.1 Silicon Isotope Work

This thesis was aimed originally at determining whether the Boone cherts were dominantly organically precipitated or inorganically precipitated through the dissolution and reprecipitation of volcanic ash by utilizing silicon isotope ratios. Samples were processed, but accurate data were unable to be obtained on the mass spectrometer at the University of Arkansas. This appendix provides a summary of that work and the goals of the original project. The objective of was to use silicon isotopes along with trace element concentrations to gain a more complete geochemical understanding of the interval, and ultimately determine: 1) whether silicon isotopes suggest a volcanogenic source for the silica of the Lower Mississippian Boone Formation cherts as well as that of the Arkansas Novaculite, and 2) whether both units reflect the same volcanogenic source. Silicon isotopes are fractionated during biomineralization of opal (De La Rocha 2003). A sixfold greater range in the $\delta^{30}Si$ values has been observed for biogenic versus abiotic geologic samples (Douthitt 1982). Therefore, if the silica in the chert were biogenic, the $\delta^{30}Si$ values would be more negative and show greater variability than if it is volcanogenic. If the samples indicate a volcanogenic source, it is hypothesized that the silica source must be volcanic ash produced by an island arc associated with the Ouachita Orogeny.

A total of 32 samples were prepared for analysis from localities in the southern midcontinent, including Bella Vista, AR; Caddo Gap, AR; Pineville, MO; Branson, MO; and Kansas, OK (Figure 1). This sampling includes 12 from penecontemporaneous chert, ten from later diagenetic chert, and ten from novaculite. These samples were prepared by cutting one-centimeter thick slabs of rock, which were then wrapped and broken to retrieve innermost, unaltered pieces of rock. These chips were then powdered using a shatterbox, and dissolved using HF, HCl, and HNO_3 acid. Each sample was analyzed for trace elements using the

Quadrupole Inductively Coupled Plasma Mass Spectrometer (Q ICP-MS) at the University of Arkansas.

Samples for silicon isotope analysis were processed in five rounds of eight samples using the sodium hydroxide digestion method outlined in van den Boorn et al. (2006). 2 mg of powdered whole rock samples were weighed out on filter paper, transferred into PTFE liners. 60 mg of NaOH were added to each sample, and PTFE liners were enclosed in Parr acid digestion vessels (Parr "bombs"). Each Parr bomb was transferred to the oven and heated for 3 days at 200°C. After cooling, the Parr bombs were opened up to reveal the digested silicates in solid form. 1 mL of triple distilled Savillex water was added to each sample, prompting partial dissolution of each sample. PTFE liners were put on a hot plate at 80°C for approximately one hour to get each sample into solution. Two samples, AGV and BHVO developed a dark residue, which was consistent with the van den Boorn et al. (2006) study. Samples were transferred (residue included) into Savillex PFE vials. Silicon isotope analysis was attempted using a Multicollector ICP-MS. Due to unresolved interference issues, accurate data was not obtained during analysis of the silicon isotope standard (NBS 28). It is the hope of this author that the processed samples from this original thesis projects will be successfully analyzed in the future with advancement of analytical techniques at the University of Arkansas.